Transcriptomic and physiological analysis reveal phytohormone and phenylpropanoid biosynthesis in root of Cynanchum auriculatum

Miao Sun (nixbio@sci.edu.rs)
Yancheng Teachers University
Zhi-Peng Zhu
Yancheng Teachers University
Jian-Xiang Yu
Yancheng Teachers University
Ke-Xin Wu
Yancheng Teachers University
Yao-Xian Guo
Yancheng Teachers University
Min Shen
Yancheng Teachers University
Fang-Fang Liu
Yancheng Teachers University
Xin-Hui Tang
Yancheng Teachers University
Yi-Jun Kang
Yancheng Teachers University

Research Article

Keywords: Cynanchum auriculatum, Tuberous root, Transcriptomic analysis, Phytohormone, Lignin, Flavonoids

Posted Date: August 9th, 2022

DOI: https://doi.org/10.21203/rs.3.rs-1923730/v1

Version of Record: A version of this preprint was published at Plant Growth Regulation on February 10th, 2023. See the published version at https://doi.org/10.1007/s10725-022-00953-3.

Abstract

Baishouwu (*Cynanchum auriculatum*), a medicinal and food dual-use plant, has been cultivated for centuries and is favored by consumers. *C. auriculatum* tuberous roots contain large amounts of flavonoids, lignin, and other nutrients. However, the developmental characteristics and phenylpropanoid metabolic mechanism in *C. auriculatum* have not been clarified. Here, *C. auriculatum* tuberous roots were observed in three developmental stages, compared with root forming stage (S1), there were significant morphological differences in root expanding stage (S2) and harvest stage (S3). Through Illumina HiSeq2500, nine transcriptomic libraries were constructed for transcriptomic analysis. 28,926 DEGs were activated during the development of *C. auriculatum* tuberous root, and many DEGs were enriched in 'phytohormone signal transduction' and 'phenylpropanoid biosynthesis'. The analysis of phytohormone content and gene expression revealed that, auxin, cytokinin, and ethylene participated in the regulation of *C. auriculatum* tuberous root development. With phloroglucinol staining, it was observed that lignified cells were mainly distributed in the central xylem at S1, followed by ring-like structure formation in S2, and finally formed the connecting rays between the xylem and the phloem in S3. Lignin content increased at S2 and then decreased at S3, and the expression of lignin synthesis genes also presented a similar trend. Total flavonoids content showed a gradually increasing trend, and the expression of flavonoid synthesis genes was also gradually up regulated. *C. auriculatum* might divert the precursors to the flavonoid synthesis pathway by reducing the activity of key enzymes in lignin synthesis, resulting in the reduction of lignin content and the promotion of flavonoid synthesis. This study provided a basis for the developmental mechanism of *C. auriculatum* and the further utilization of *C. auriculatum* tuberous roots.

Introduction

Baishouwu (*Cynanchum auriculatum*), a plant belonging to *Asclepiadaceae* family, is distributed in China, Japan, and Korea (Chen et al., 2019). In China, *C. auriculatum* is widely cultivated in Shandong, Jiangsu, and Anhui provinces, and 95% of *C. auriculatum* products are produced from Binhai County, Jiangsu Province. As a medicinal and food dual-use plant material, tuberous root of *C. auriculatum* has been used by local consumers as a health food for decades (Qi et al., 2009). Recent research has shown that, the biomedical function of *C. auriculatum* is due to the natural active substances' rich in its tuberous root, including 2,4-dihydroxyacetophenone, 4-hydroxyacetophenone, cynandione, bungeiside, and so on (Li et al., 2013; Uchikura et al., 2018; Zhang et al., 2009). At the same time, a variety of active compounds impart pharmacological functions to *C. auriculatum* products, such as polysaccharide fraction against hydrogen peroxide-induced oxidative stress (Chai et al., 2018), C21 steroidal glycosides against H_2O_2-induced damage (Zhang et al., 2019), and aglycone caudatin against cancer cell (Bailly, 2021). However, the developmental mechanism of *C. auriculatum* tuberous root and the accumulation mechanism of important active substances have not been elucidated, which hinders the basic research and breeding engineering of *C. auriculatum*.

In plants, lignin is a polymer compound formed by the differentiation of monomers synthesized through the phenylpropanoid pathway, and it plays an important role in the growth and development mechanism

(Ralph et al., 2019). As the main structural component of the cell wall in terrestrial plants, lignin maintains the hardness of the xylem, promotes water transportation, and blocks the infection of insects and pathogens (Liu et al., 2018). In certain types of plants, lignin has a significant effect on the germination mechanism of seeds, and the reduction of lignin content in the seed coat seriously affects the germination rate and growth rate (Liang et al., 2006; Mir Derikvand et al., 2008; Vanholme et al., 2012). In anthers, the absence of lignin resulted in severe inhibition of male sterility and loss of apical dominance, which ultimately manifested as stunted plant growth (Schilmiller et al., 2009; Thévenin et al., 2011). In the development of tuberous root, lignin is primarily dedicated to the formation of xylem parenchyma cells that store starch (Zierer et al., 2021). However, different from the root development of tree species, high lignin content is not conducive to the storage organ formation of root plant species, as reported in *Ipomoea batatas* (Firon et al., 2013; Sojikul et al., 2015). In the process of storage root formation, the inhibition of lignin synthesis promoted the proliferation of xylem and cambium cells, which in turn led to the thickening and growth of storage roots (Noh et al., 2013). Therefore, appropriate lignin content is of great significance for the growth and development of tuberous root plants.

Flavonoid is an important active substance of *C. auriculatum*, which contributes to plant development (Dong and Lin, 2021) and has great potential in the fields of food health and pharmaceuticals (Parhi et al., 2020). Like the synthesis mechanism of lignin, the synthesis of flavonoids (tannins, anthocyanins and flavonols) is also through the phenylpropanoid pathway (Liu et al., 2021). Some researchers have found that, the changes in the expression levels of upstream structural genes (*PAL*, *C4H*, and *4CL*) simultaneously affected the synthesis of tannins, anthocyanins, and lignin (Schilmiller et al., 2009; Thévenin et al., 2011). The contents of phenolic acids and lignin were increased in transgenic *N. tabacum* and *A. thaliana* overexpressing *CsHCT*, while the content of flavonol glycosides was decreased (Chen et al., 2021). Meanwhile, some transcription factors affected the biosynthesis of lignin and flavonoids by regulating the expression of structural genes, and direct redistribution of carbon metabolism in plants (Bhargava et al., 2010; Deluc et al., 2008; Fornalé et al., 2010). In *Populus L*., the overexpression of *MYB6* reduced secondary cell wall deposition and significantly promoted the accumulation of anthocyanins and procyanidins (Wang et al., 2019). Hence, the study of the flavonoid biosynthesis pathway in *C. auriculatum* tuberous root can not only clarify the accumulation mechanism of flavonoids, but also be beneficial to explore the transformation rule of lignin content.

In this study, tuberous roots at three developmental stages (S1: root forming stage, S2: root expanding stage, and S3: harvest stage) were analyzed. We analyzed the enrichment pathways and expression levels of DEGs during the development of *C. auriculatum* tuberous root by RNA-Seq. Furthermore, through integrated analysis of phytohormones, lignin, and flavonoids, and related genes involved in their metabolic pathways, the associated between metabolites and genes was explained to provide valuable information for revealing the development characteristics of *C. auriculatum* tuberous root. This study aimed to elucidate the mechanism of tuberous root development and explore the regulatory mechanism of phytohormones, lignin, and flavonoids in *C. auriculatum*.

Materials And Methods

2.1 Plant materials

Annual *C. auriculatum* (genotype Yanwu 1406, a local variety of Yancheng) plant materials were grown (since 10 May 2021) in the experimental field of Yancheng Xinyang Agricultural Experiment Station (120.16 E, 33.52 N), Yancheng, Jiangsu Province of China. *C. auriculatum* tuberous roots were sampled at three development stages, including root forming stage (S1, on 15 Sept 2021), root thickening stage (S2, on 15 Oct 2021), and root harvest stage (S3, on 15 Nov 2021), referring to the agronomic details of *Cassava* (Yao et al., 2017). *C. auriculatum* materials, with three biological replicates for further analysis, were washed carefully and stored in the ultra-low temperature freezer of -80 °C (Fig. 1). Part of the samples was then sent to Guangzhou Gene Denovo Biological Technology Co., Ltd for high-throughput transcriptomic sequencing, and the others were kept for physiological analysis.

2.2 Phytohormone extraction and content determination

1.0 g of *C. auriculatum* root samples were added with 2.0 mL of extraction solution (100 % methanol) and grounded with liquid nitrogen. After standing at 4 °C for 4 h, the supernatant was collected after centrifugation at 4000 rpm for 15 min. Then, after repeating the above step once more, the supernatant was combined for C18 solid phase extraction. Afterward, the supernatant was eluted by 100 % methanol and purified using the 0.45 μm microporous filter for subsequent phytohormone content determination.

The endogenous contents of Indole-3-acetic acid (IAA), cytokinin (CK), and ethylene (ETH) were determined with phytohormone ELISA assay kits (Catalog No. QS42270 for IAA, Catalog No. QS441290 for CK, and Catalog No. QS49937 for ETH), respectively. And these ELISA kits were purchased from Beijing Qisong Biotechnology Co., LTD.

2.3 Phloroglucinol staining of lignified tissue and lignin content determination in *C. auriculatum* tuberous root

The chemical staining of lignified tissue of *C. auriculatum* tuberous root referred to the method described by Sun et al. (Sun et al., 2021) with minor modifications. The samples were cut longitudinally into 2.0 mm slices from the midsection of tuberous roots. The slices were immersed in the 15.0 % phloroglucinol solution for 5.0 min, and then added with 3.0 mL of 36.0 % hydrochloric acid for color reaction. The red-dyed tuberous root slices were photographed with the EOS 1300D digital camera, the cell structure was observed and photographed using the MOTIC BA200 optical microscope.

Besides, lignin content of *C. auriculatum* tuberous root was assayed with Lignin Content Detection ELISA Kit (Catalog number: BC4200, purchased from Beijing Solarbio Technology Co., Ltd.) and determined with UV spectrophotometry at A_{280}.

2.4 Total flavonoids content determination of *C. auriculatum* tuberous root

Total flavonoids content of *C. auriculatum* tuberous root was assayed and analyzed according to the colorimetric method of sodium nitrite-aluminum nitrate-sodium hydroxide (Chen et al., 2020). Briefly, a standard curve was prepared with rutin (Catalog number: R8170, purity ≥ 95.0 %, purchased from Beijing Solarbio Technology Co., Ltd.) as the standard sample. 1.0 mL of *C. auriculatum* tuberous root powder (2.0 mg/mL) was added with 1.0 mL of sodium nitrite solution (50.0 mg/mL), 1.0 mL of aluminum nitrate solution (100.0 mg/mL), 4.0 mL of sodium hydroxide solution (200.0 mg/mL), and 3.0 mL of 37.0 % ethanol. After static settlement for 15.0 min, the absorbance of the mixture was measured at A_{510}.

2.5 mRNA extraction and high-throughput transcriptomic library sequencing

The mRNA of *C. auriculatum* tuberous root was extracted by TIANSeq mRNA Capture Kit (Catalog number: NR105-01, purchased from Beijing Tiangen Biotechnology Co., Ltd.). To ensure the quality of sequencing result, the construction quality of the library was strictly checked, and the detection standards were as follows: agarose gel electrophoresis for the analysis of RNA integrity and DNA contamination, NanoPhotometer spectrophotometer for the determination of RNA purity, Qubit2.0 Fluorometer for the accurate quantification of RNA concentration, and Agilent 2100 bioanalyzer for the precise detection of RNA integrity.

Using random oligonucleotides as primers, the first strand of cDNA was synthesized in the M-MuLV reverse transcriptase system. Next, RNA degradation and the second strand of cDNA synthesis occurred. The purified double-stranded cDNA was end-repaired and connected to a sequencing adapter. AMPure XP beads were used to screen cDNAs and purify the PCR products. Finally, high-throughput transcriptomic libraries were obtained by Illumina HiSeq2500. In addition, the quality inspection of the transcriptomic library was evaluated according to the manual of DNA 1000 Assay Kit (Catalog number: 5067-1504, purchased from USA Agilent Technology Co., Ltd.).

2.6 Bioinformatics analysis of *C. auriculatum* transcriptome

The original reads were further filtered by fastp (version 0.18.0) to obtain high-quality clean reads (Chen et al., 2018). Through StringTie (version 1.3.1), the mapped reads of each sample were assembled (Pertea et al., 2015). The analysis of differentially expressed genes (DEGs) between different groups was performed with DESeq software (Love et al., 2014). Principal component analysis (PCA) was performed with R package gmodels (http://www.rproject.org/org/). Gene Ontology (GO) analysis (Ashburner et al., 2000) was performed by mapping DEGs to the Gene Ontology database (http://www.geneontology.org/). Kyoto Encyclopedia of Genes and Genomes (KEGG) analysis was performed with edgeR software (Robinson et al., 2010).

2.7 qRT-PCR analysis of DEGs from *C. auriculatum* transcriptome

To verify the reliability of *C. auriculatum* transcriptomic profiling data, qRT-PCR was carried out by SYBR® Premix Ex Taq™ (Catalog number: RR820Q, purchased from Beijing TaKaRa Biotechnology Co., Ltd.) and performed on Thermal Cycler Dice™ Real Time System *Lite* (Code No. TP700/TP760, purchased

from Beijing TaKaRa Biotechnology Co., Ltd.). Sixteen genes related to starch synthesis, lignin synthesis, flavonoids synthesis, and auxin signaling, respectively, were selected for qRT-PCR assay, and *CaActin7* was used as the reference gene.

The relative expression levels of selected genes were calculated through the $2^{-\Delta\Delta CT}$ method (Livak and Schmittgen, 2001). The primers used in this study were designed by NCBI primer design online tool (https://www.ncbi.nlm.nih.gov/tools/primer-blast/) and synthesized by Anhui General Biol Co., Ltd. The nucleotide sequences and amplification characteristics of the primers had been shown in Supplementary Table 1.

In addition, to ascertain whether the correlation between qRT-PCR analysis data and FPKM values from RNA-Seq was significant, Ozone correlation analysis was applied with GraphPad Prism 8.0 software.

2.8 Statistical Analysis

All experiments were performed within three or more biological replicates to eliminate errors. The data was statistically analyzed and graphed by GraphPad Prism 8.0 software, and the significant difference analysis was measured with One-Way or Two-Way ANOVA multiple comparison (*P* value < 0.05 or 0.01).

Results

3.1 Sample relationship analysis of *C. auriculatum* tuberous root

To investigate the developmental characteristics of *C. auriculatum* tuberous root, the samples of three development stages were observed and analyzed. It could be observed that, the samples (S1 in Sept, S2 in Oct, and S3 in Nov) exhibited obvious morphological changes (Fig. 1A). Compared with S1, average root length (14.12 cm of S2, 23.63 cm of S3) and root weight (22.59 g of S2, 54.49 g of S3) were significantly higher in later developmental stages (Fig. 1B).

In the meantime, the analysis results of PCA, sample clustering, violin plot, and correlation heat map showed that (Fig. 2), there was significant variability among the samples collected in different developmental stages, and the three biological replicates of the samples were quite reproducible.

3.2 Quality assessment and basic information of *C. auriculatum* tuberous root transcriptome data

C. auriculatum tuberous root samples at three development stages, with three biological replicates, were used for the construction of nine transcriptomic libraries, including S1-Sept-1, S1-Sept-2, S1-Sept-3, S2-Oct-1, S2-Oct-2, S2-Oct-3, S3-Nov-1, S3-Nov-2, and S3-Nov-3. The transcriptomic libraries had been uploaded in NCBI SRA database (https://www.ncbi.nlm.nih.gov/sra/), which were named as SRX14155705 (S1-Sept-1), SRX14155706 (S1-Sept-2), SRX14155707 (S1-Sept-3), SRX14155708 (S2-Oct-1), SRX14155709 (S2-Oct-2), SRX14155710 (S2-Oct-3), SRX14155711 (S3-Nov-1), SRX14155712 (S3-Nov-2), and SRX14155713 (S3-Nov-3).To reduce the interference caused by invalid data, data filtering was performed on the original data, and the obtained clean reads were as follows: 5,792,103,000 bp of

S1-Sept-1, 6,402,806,400 bp of S1-Sept-2, 6,158,593,800 bp of S1-Sept-3, 5,621,652,900 bp of S2-Oct-1, 6,548,790,900 bp of S2-Oct-2, 7,550,866,800 bp of S2-Oct-3, 7,554,501,300 bp of S3-Nov-1, 7,505,005,500 bp of S3-Nov-2, 8,607,777,900 bp of S3-Nov-3. The balance analysis of base composition showed that, the quality of the transcriptome library was high, which was beneficial to the accuracy of subsequent analysis (Supplementary Table 2).

Using our published full-length *C. auriculatum* transcriptomic database (NCBI accession number: SRX10889362) as the reference, sequence alignment and quantification were performed by RSEM, and the gene detection in each sample was counted (Supplementary Table 3). The reads on the isoform of our libraries were evenly distributed in each part of *C. auriculatum* gene, indicating that the randomness of mRNA interruption was satisfactory (Supplementary Figure 1). In addition, FPKM distribution and expression violin plot of all samples showed high gene expression abundance and high data density at corresponding sites in these transcriptome libraries (Supplementary Figure 2).

3.3 DEGs Enrichment analysis of *C. auriculatum* tuberous root during development

To investigate the changes at the molecular level during the development of *C. auriculatum* tuberous root, DEGs enrichment of the nine transcriptomic libraries was analyzed. Taking genes with FDR<0.05 and $|\log^2 FC|>1$ as significantly different genes, the comparison between groups showed that there was a total of 14,944 DEGs (7,454 of up-regulated, 7,490 of down-regulated) between S1 *vs* S2, 14,496 DEGs (9,962 of up-regulated, 4,534 of down-regulated) between S2 *vs* S3, 20,016 DEGs (12,890 of up-regulated, 7,126 of down-regulated) between S1 *vs* S3 (Fig. 3A). In addition, difference comparison volcano plot (Fig. 3B), difference comparison cluster heatmap (Fig. 3C), and Venn diagram showed 28,926 of DEGs among the groups of S1, S2, and S3, indicating that the expression of these genes was affected by the development of *C. auriculatum* tuberous root.

Gene Ontology (GO) enrichment was analyzed to comprehensively characterize the properties of genes and gene products in *C. auriculatum* tuberous root during development. The comparison results (S1 *vs* S2, S2 *vs* S3, S1 *vs* S3) had been shown in Supplementary Fig. 3, taking S1 *vs* S2 as an example, in ‘Biological Process’, the top 5 GO enrichment classifications included ‘metabolic process’ (403 of up-regulated, 213 of down-regulated), ‘single-organism process’ (275 of up-regulated, 186 of down-regulated), ‘cellular process’ (205 of up-regulated, 140 of down-regulated), ‘localization’ (58 of up-regulated, 36 of down-regulated), and ‘biological regulation’ (19 of up-regulated, 58 of down-regulated). In ‘Cellular Component’, the top 5 enrichment classifications included ‘cell’ (148 of up-regulated, 102 of down-regulated), ‘cell part’ (148 of up-regulated, 102 of down-regulated), ‘membrane’ (90 of up-regulated, 70 of down-regulated), ‘organelle’ (52 of up-regulated, 79 of down-regulated), and ‘extracellular region’ (34 of up-regulated, 1 of down-regulated). Besides, in the enrichment of ‘Molecular Function’, ‘catalytic activity’ (347 of up-regulated, 279 of down-regulated), ‘binding’ (212 of up-regulated, 197 of down-regulated), ‘transporter activity’ (23 of up-regulated, 29 of down-regulated), ‘structural molecule activity’ (12 of up-regulated, 0 of down-regulated), and ‘molecular function regulator’ (3 of up-regulated, 3 of down-regulated) were the top 5 enrichment classifications. In S2 *vs* S3, in ‘Biological Process’, the top 5

GO enrichment classifications included ‘metabolic process’ (260 of up-regulated, 233 of down-regulated), ‘single-organism process’ (217 of up-regulated, 160 of down-regulated), ‘cellular process’ (222 of up-regulated, 98 of down-regulated), ‘localization’ (74 of up-regulated, 20 of down-regulated), and ‘biological regulation’ (68 of up-regulated, 14 of down-regulated). In ‘Cellular Component’, the top 5 enrichment classifications included ‘cell’ (139 of up-regulated, 73 of down-regulated), ‘cell part’ (139 of up-regulated, 73 of down-regulated), ‘membrane’ (95 of up-regulated, 90 of down-regulated), ‘organelle’ (54 of up-regulated, 50 of down-regulated), and ‘membrane part’ (36 of up-regulated, 54 of down-regulated). And in the enrichment of ‘Molecular Function’, ‘catalytic activity’ (310 of up-regulated, 194 of down-regulated), ‘binding’ (276 of up-regulated, 119 of down-regulated), ‘transporter activity’ (15 of up-regulated, 39 of down-regulated), ‘signal transducer activity’ (19 of up-regulated, 5 of down-regulated), and ‘molecular transducer activity’ (13 of up-regulated, 3 of down-regulated) were the top 5 enrichment classifications.

Through KEGG pathway significant enrichment, the main biochemical metabolic pathways and signal transduction pathways in *C. auriculatum* tuberous root involved in DEGs were determined. The comparison results showed that (Supplementary Fig. 4), in the comparison of S1 *vs* S2, the top 5 KEGG enrichment classifications included ko01100 ‘Metabolic pathways’ (5105 DEGs in 2169 KEGG pathways), ko01110 ‘Biosynthesis of secondary metabolites’ (2770 DEGs in 1372 KEGG pathways), ko01230 ‘Biosynthesis of amino acids’ (830 DEGs in 528 KEGG pathways), ko01200 ‘Carbon metabolism’ (854 DEGs in 377 KEGG pathways), and ko03010 ‘Ribosome’ (481 DEGs in 334 KEGG pathways). In the comparison of S2 *vs* S3, the top 5 enrichment classifications changed to ‘Metabolic pathways’ (5105 DEGs in 1660 KEGG pathways), ‘Biosynthesis of secondary metabolites’ (2770 DEGs in 924 KEGG pathways), ko04075 ‘Plant hormone signal transduction’ (594 DEGs in 258 KEGG pathways), ko03040 ‘Spliceosome’ (690 DEGs in 251 KEGG pathways), and ‘Biosynthesis of amino acids’ (830 DEGs in 228 KEGG pathways).

In addition, combining the results of GO and KEGG enrichment analysis, we found that a large number of DEGs favored enrichment of ‘Plant hormone signal transduction’ and ‘Phenylpropanoid biosynthesis’, which indicated that phytohormones and phenylpropane metabolites played critical roles in the develop of *C. auriculatum* tuberous root.

3.4 Plant hormones involved in root develop of *C. auriculatum*

As phytohormones play a critical role in mediating plant growth, development, and response to environmental factors, DEGs related to phytohormone signal transduction were sought out and listed. There were 564 DEGs involved in the KEGG pathway of ‘Plant hormone signal transduction’, which could be divided into 44 families. The results showed that (Fig. 4), the top 10 families included ARF (73 of DEGs, 12.94 %), EIN (59 of DEGs, 10.46 %), AHK (47 of DEGs, 8.33 %), IAA (42 of DEGs, 7.45 %), ETR (33 of DEGs, 5.85 %), LAX (32 of DEGs, 5.67 %), NPR (30 of DEGs, 5.32 %), BSK (21 of DEGs, 3.72 %), ARR (16 of DEGs, 2.84 %), and CTR (16 of DEGs, 2.84 %). Among them, IAA, TIR, LAX, ARF, and GH3 were involved in IAA biosynthesis, transport, and signal transduction, respectively. ARR was responsible for CK signal transduction, EIN, ETR, and CTR were involved in ETH signal transduction. In addition, BSK, NPR and GAI

participated in the signal transduction of brassinolide, salicylic acid, and gibberellin, respectively. These results indicated phytohormones, including auxin, cytokinin, ethylene, brassinolide, salicylic acid, and gibberellin, were important for the development of *C. auriculatum* tuberous root. In addition, to explore the role of phytohormone in root development of *C. auriculatum*, phytohormones (IAA, CK, and ETH) content and their related gene expression levels were assayed.

The crucial role of auxin has been proved in many tuber and storage root crops (Kondhare et al., 2021). Compared with S1, IAA content of S2 significantly increased by 17.94 %, while IAA content increased by 15.21 % in S3 (Fig. 5A). At the same time, FPKM values of IAA synthesis and signaling genes, such as tryptophan aminotransferase-1 (PB.34545.1, *CaTAA1*), anthranilate synthase alpha subunit (PB.19512.1, *CaASA*), *CaYUC*(PB.24614.1), gretchen hagen 3.1 (PB.18264.1, *CaGH3.1*), like auxin resistant (PB.20718.1, *CaLAX*), *CaIAA* (PB.14080.1, PB.22449.1), auxin resistant (PB.18013.1, *CaAUX*), like auxin (PB.27159.1, *CaLAX*), pin-formed (PB.15955.1, *CaPIN1*; PB.12675.1, *CaPIN3*), auxin response factor (PB.6875.1, *CaARF3*; PB.11636.1, *CaARF6*; PB.20529.1, *CaARF19*), whose change trends were generally similar to IAA content (Fig. 5B).

By interfering with auxin transport, CKs promoted PIN protein degradation and regulated root development (Jing and Strader, 2019). In the present work, compared with S1, CK content showed a change trend similar to IAA content, which significantly increased in S2 (increased by 70.26 %) and decreased in S3 (Fig. 6A). Meanwhile, CK synthesis, transport, and signaling genes, including E3 ubiquitin-protein ligase (PB.29516.1, *CaLOG2*), purine permease (PB.33715.1, *CaPUP1*; PB.30852.1, *CaPUP3*; PB.23081.1, *CaPUP21*), ABC transporter G family member (PB.12451.1, *CaABCG14*), histidine kinase (PB.36978.1, *CaAHK4*), type-A response regulator (PB.32971.1, *CaARR9*; PB.2389.1, *CaARR15*), whose FPKM values also followed the expected trend with elevated expression in S2 and decreased in S3 (Fig. 6B).

Studies have indicated that ethylene shows significant inhibition of the growth of primary roots (Qin et al., 2019a; Qin and Huang, 2018). Here, it has been found that during tuber root development of *C. auriculatum*, ETH content decreased from 86.64 ng/kg FW (S1) to 42.21 ng/kg FW (S3) (Fig. 7A). And then, ETH biosynthesis and signaling genes, including acetyl-coenzyme A synthetase (PB.11689.1, *CaACS*), 1-aminocyclopropane-1-carboxylic acid oxidase (PB.2145.1, *CaACO*), ethylene receptor (PB.10599.1, *CaETR1*; PB.2607.1, *CaETR2*), ethylene insensitive 3 (PB.10463.1, *CaEIN3*), ethylene responsive factor (PB.2298.1, *CaERF4*; PB.28708.1, *CaERF110*; PB.33534.1, *CaERF5*), whose expression levels were consistently reduced (Fig. 7B).

3.5 Changes in lignin biosynthesis during tuberous root development of *C. auriculatum*

To explore the lignin biosynthesis mechanism of *C. auriculatum* tuberous root, *C. auriculatum* tuberous root slices at three developmental stages were excised for chemical staining and observed by light microscopy. The tuberous root slices stained with phloroglucinol-hydrochloric acid solution showed that, at tuberous root forming stage (Fig. 8A, D), lignified cells were mainly distributed in the central xylem of the longitudinal section of *C. auriculatum* tuberous root. As the tuberous root gradually expanded

and thickened, the expanded central xylem tore the surrounding endothelial cells, and the lignified cells were observed to form a ring-like structure (Fig. 8B, E). Finally, at *C. auriculatum* tuberous root harvest stage, the core part was basically devoid of lignified cells, and the rays composed of lignified cells extended from the xylem to the phloem, ensuring the connection between the two transport systems (Fig. 8C, F).

The determination of lignin content indicated that (Fig. 9A), compared with the lignin content of S1 (18.54 mg/g FW), the lignin content of S2 significantly increased to 26.97 mg/g FW and decreased slightly at the development stage of S3 (20.41 mg/g FW). In addition, structural genes involved in the lignin biosynthesis mechanism were identified, and their expression levels were analyzed. Based on RNA-Seq data, the key genes in phenylpropanoid pathway, *CaPAL* (PB.11234.1), *CaC4H* (PB.26497.1) and *Ca4CL* (PB.22367.2), whose FPKM values tended to increase throughout the developmental stages. However, the FPKM values of structural genes all peaked at the stage of S2, and then showed a decline in S3 (Fig. 9B). Compared with the expression level at S1, the expression level of *CaHCT* (PB.6659.1) was increased by 2.63 times at S2 but increased by 1.37 times at S3, the expression level of *CaC3H* (PB.26740.1) was increased by 2.08 times at S2 but increased by 1.27 times at S3, and the expression level of *CaCSE* (PB.2200.1) was increased by 6.33 times at S2 but increased by 4.01 times at S3.

3.6 Enhancement of Flavonoids biosynthesis during tuberous root development of *C. auriculatum*

In this study, total flavonoids content had been determined to preliminarily explore the synthesis mechanism of flavonoids in *C. auriculatum* tuberous root. The data showed that (Fig. 10A), compared with the flavonoids content of S1 (6.23 mg/g), the flavonoids content was significantly higher in S2 (7.41 mg/g) and S3 (7.89 mg/g).

Furthermore, based on the data of the nine transcriptomic libraries, the FPKM values of structural genes involved in flavonoids biosynthesis pathway showed that (Fig. 10B), the relative expression levels of *CaCHS* (PB.2117.1), *CaCHI* (PB.2442.1), *CaF3H* (PB.28001.1), *CaDFR* (PB.33673.1), *CaANS* (PB.32955.1), *CaFLS* (PB.33009.1), *CaANR* (PB.2294.1), *CaF3'H* (PB.1898.1), *CaLAR* (PB.32826.1), and *CaUFGT* (PB.29841.1) all showed varying degrees of an upward trend, especially *CaCHI*, *CaFLS*, *CaLAR*, and *CaUFGT*. Interestingly, the variation trend in the expression profiles of these genes were both significantly and positively associated with the changes in the total flavonoids content of *C. auriculatum* tuberous root at different developmental stages.

3.7 Expression profile verification of *C. auriculatum* DEGs by qRT-PCR

To verify the reliability of DEGs expression profiles from the nine *C. auriculatum* transcriptomic libraries, sixteen DEGs, which are related to starch synthesis (PB.11739.1: *CaSS4*, PB.11812.1: *CaSS3*, PB.39555.1: *CaSBE1*; PB.9531.1, *CaSUS2*), lignin synthesis (PB.1851.1: *CaCCR*, PB.28934.1: *CaCAD*, *CaCSE*; PB.21485.1, *CaPOD*), flavonoids synthesis (*CaCHS*, *CaCHI*, *CaDFR*, *CaFLS*) and auxin signaling (PB.18264.1: *CaGH3.1*; PB.20718.1, *CaLAX2*; PB.6875.1, *CaARF3;* PB.12675.1, *CaPIN3*), respectively, were

selected for qRT-PCR validation, and *CaAct7* (PB.15198.1) was used as reference gene to control the variable.

According to the heatmap analysis of FPKM values from RNA-Seq data (Fig. 11A) and $\log_2$ (ratio) values from qRT-PCR analysis (Fig. 11B), the expression of selected genes showed similar change trends. For example, in starch metabolism, compared with S1, the expression level of *CaSS4* increased by 1.35 times in S2 and 3.86 times in S3, the expression level of *CaSS3* decreased by 0.06 times in S2 and increased by 0.26 times in S3, the expression level of *CaSBE1* decreased by 0.67 times in S2 and 0.86 times in S3, and the expression of *CaSUS2* increased by 1.43 times in S2 and 2.44 times in S3. In the pathway of IAA signal transduction, compared with S1, the expression of *CaIAA9* increased by 0.33 times in S2 and decreased by 0.13 times in S3, the expression of *CaLAX2* increased by 0.30 times in S2 and decreased by 0.37 times in S3, the expression of *CaARF3* increased by 0.72 times in S2 and decreased by 0.36 times in S3, and the expression of *CaPIN3* showed a 92.17% increase in S2 and a 251.49% increase in S3.

In addition, Ozone correlation analysis was performed with GraphPad 8.0 software. The results demonstrated that, the R square between FPKM value and qRT-PCR value was 0.7107, and the *P* value was less than 0.001, indicating that the values of qRT-PCR and FPKM were significantly correlated (Fig. 11C), and the results of transcriptomic sequencing were credible.

Discussion

4.1 The developmental characteristics of *C. auriculatum* tuberous root revealed by RNA-Seq at the molecular level

C. auriculatum tuberous root provides a variety of carbohydrates, proteins, and vitamins for human health. At the same time, the high levels of ascorbic acid and carotenoids make the root barks appear to be bright yellow (Zierer et al., 2021), which could also be observed on the root bark of the samples we collected (Fig. 1A). During the root forming stage (S1), expanding stage (S2), and harvest stage (S3), the morphology of *C. auriculatum* tuberous roots changed obviously (Fig. 1A), which was embodied in average root length and average root weight (Fig. 1B).

Along with development progresses, multiple metabolic processes were activated in *C. auriculatum* tuberous root (Supplementary Fig. 3). For example, the KEGG pathway of ‘Starch and sucrose metabolism’ was found to be enriched in a lot of DEGs (Supplementary Fig. 4). Carbohydrate metabolism plays an important role in the development of tuberous root in plants (Mehdi et al., 2019). Root crops and tuber crops use starch stored in the roots as an energy reserve to support growth and development (Kondhare et al., 2020). Here, the values of FPKM and qRT-PCR showed that the expression levels of genes encoding enzymes related to starch metabolism, including *SS4* (Lu et al., 2018), *SS3* (Gámez-Arjona and Mérida, 2021) were up-regulated (Fig. 11), and the expression of *SBE1* (Utsumi et al., 2021), the gene inhibiting digestion-resistant starch synthesis (Schwall et al., 2000), was down-regulated. Besides, similar results had been partly confirmed in *Ipomoea batatas* (Utsumi et al., 2020).

4.2 The role of phytohormones in *C. auriculatum* tuberous root during development

Phytohormones are actively involved in the changes of tuberous root morphology and the accumulation of starch and amino acids (Sun et al., 2019), such as IAA (Kondhare et al., 2021), GA (Zhou et al., 2021), CK (Jang et al., 2015), and ETH (Liu et al., 2017).

Different concentrations of auxin controlled multiple cell activities, including secondary wall formation, cell expansion and division (Fischer et al., 2019). In *Ipomoea batatas*, it was speculated that auxin triggered the process of vascular cambium formation in the basal root system (Rüscher et al., 2021). At the same time, genes related to auxin transduction, such as *ARF* (Roosjen et al., 2018), *SAUR* (Wang et al., 2020), and *GH3* (Zou et al., 2019), were found to regulate the function of auxin protein. In this study, in contrast to root forming stage (S1), IAA accumulated in root expanding stage (S2), and there was its decay afterwards in root harvest stage (S3) (Fig. 5A). At the same time, this study also showed the same expression trend of IAA synthesis and signaling genes (Fig. 5B). Gao et al. had proved that IAA was specifically enriched in the formation and enlargement stages of subterranean organs (Gao et al., 2016). However, IAA synthesis showed a decline at root harvest stage of *C. auriculatum*, which suggested that accompanied by cell growth arrest, the last stage of tuber root development was independent of auxin effects (Kolachevskaya et al., 2015). Similar phenomenon also appeared in CK synthesis, transport, and signaling (Fig. 6), which was possibly due to CK concentrating in the meristematic region of the secondary xylem and in the phloem (Melis and van Staden, 1985). As *C. auriculatum* root developed into harvest stage (S3), the structures of xylem and phloem tended to stabilize (Fig. 8), the effect of CK would decrease or even be ignored.

It has been reported that ETH shows significant inhibition of primary root growth (Qin et al., 2019a). For example, overexpression of *OsDOF15* positively regulated primary root elongation by limiting endogenous ethylene biosynthesis (Qin et al., 2019b). In potato, exogenous ethylene affected carbohydrate metabolism to inhibit tuber sprouting through its effects on carbohydrates and key enzymes (Dai et al., 2016). Here, we found that compared with S1, some genes related to ETH synthesis and signaling were down-regulated in S2 and S3, as well as the decreasing ETH content (Fig. 7). These results suggested that tuber root formation of *C. auriculatum* was sensitive to ETH, and *C. auriculatum* promoted the enlargement and conversion of tuberous roots into storage organs by suppressing ethylene biosynthesis (Carbonnel et al., 2020) and signaling (Zhao et al., 2020).

4.3 The role of lignin in *C. auriculatum* tuberous root during development

As a type of tuberous root crop (Ma et al., 2015), the roots of *C. auriculatum* developed from adventitious roots and gradually expanded to form storage organ. Different from woody plants, the root system of tuberous root crops is mainly composed of lignified cells that store secondary metabolites, such as starch and amino acids (Villordon et al., 2014). In this study, as shown in Fig. 8, during the development of *C. auriculatum* tuberous root, lignified cells first concentrated in the central xylem of root tuber. Then, as the rate of cell division and expansion increased, more lignified cells were augmented to accommodate the expansion of the root system, and these cells formed a ring structure separated from

the central core. At tuberous root harvest stage, the vertical section of the root showed many rays connecting the xylem and phloem of *C. auriculatum* tuberous root. This morphology was similar to the study of *Manihot esculenta* (Mehdi et al., 2019), and we speculated that these rays were vascular cells formed by secondary cambium, which helped to support the central root region.

Concordantly, we found that during tuberous root development, lignin content increased firstly and then decreased (Fig. 9A). Likewise, FPKM values of lignin biosynthesis genes (*CaCCR*, *CaCAD*, *CaPOD*, etc.) from RNA-Seq showed associated changes. Notably, when the phenylpropane metabolic pathway shifted to the lignin synthesis pathway, rate-limiting enzyme genes, including *CaCSE* and *CaHCT*, were down-regulated in S3 (Fig. 9B). As reported in *Rehmannia glutinosa* (Gu et al., 2021) and *Ipomoea batatas* (Wang et al., 2016), abnormal accumulation of lignin was not conducive to tuberous root enlargement. Therefore, these results demonstrated that in the early developmental stage of *C. auriculatum* tuberous root, the lignin content gradually increased with the expansion of the tuber, but then the expression of lignin synthesis genes was down-regulated, thereby promoting the transition from tuberous roots to storage roots (Singh et al., 2020).

4.4 The biosynthesis mechanism of flavonoids in *C. auriculatum* tuberous root during development

Flavonoids have been proved to be natural antioxidants with high content and strong activity in *Cynanchum* plants (Wu et al., 2019). The biosynthesis mechanism of flavonoids has been well described in many plants (Liu et al., 2021), including critical intermediate metabolites and structural genes. Here, we found that during the development of *C. auriculatum* tuberous root, the content of total flavonoids increased from S1 to S3 stage (Fig. 10A). At the same time, the expression profiles of flavonoids biosynthesis genes in RNA-Seq and qRT-PCR showed a similar increasing trend (Fig. 10B, 11). The results suggested that during the development of *C. auriculatum*, flavonoids biosynthesis genes (*CaPAL*, *CaC4H*, *Ca4CL*, *CaCHS*, *CaCHI*, etc.) were activated, and their increased expression level induced flavonoid accumulation in *C. auriculatum* tuberous root. Besides, flavonoids have been proved to impart color to petals and promote root growth of *Nicotiana tabacum* (Park et al., 2020). It could be observed that compared with the morphology of S1, *C. auriculatum* petioles in S3 were purple-red, and the epidermis of tuberous root was bright yellow, which had obvious correlation with the accumulation of flavonoids (Fig. 1A). This also suggested that the accumulation of flavonoids promoted the coloration of *C. auriculatum* organs.

Since the biosynthesis of lignin and flavonoids are both through the phenylpropane metabolic pathway, the changes in the contents of lignin and flavonoids in plants are closely related (Vogt, 2010). In transgenic *Arabidopsis*, mutations in *CCR1*, *CAD1*, *CAD2* resulted in reduced lignin in stems and anthers, and higher levels of flavonol glycosides, sinapoyl malate, and feruloyl malate (Thévenin et al., 2011). In *Nicotiana tabacum*, ectopic expression of *AtCPC* not only reduced the content of flavonoids, but also up-regulated the expression of lignin biosynthesis genes, which in turn significantly enhanced lignin accumulation (Shi et al., 2022). As shown in Fig. 9B and Fig. 10B, the expression of *CaPAL*, *CaC4H*, and *Ca4CL* were up-regulated during the development of *C. auriculatum* tuberous root, but at S3 stage, it

was found that the expression of lignin biosynthesis genes, particularly rate-limiting enzyme coding genes (*CaCSE*, *CaHCT*, and *CaCCR*), was suppressed, and the expression of flavonoids biosynthesis genes continued to be enhanced. These results suggested that the decreased activities of the key enzymes in lignin synthesis diverted the precursors to flavonoids synthesis pathway, resulting in reduced lignin content and continuous flavonoids accumulation of *C. auriculatum* tuberous root.

Conclusion

Tuberous root development is a critical agronomic trait affecting in *C. auriculatum*. In this study, *C. auriculatum* tuberous root (S1 in Sept, S2 in Oct, and S3 in Nov) exhibited significant phenotypic differences in root length and root weight. Based on Illumina HiSeq2500, nine high-quality RNA-Seq libraries were constructed for transcriptomic analysis. Many DEGs were identified among the groups of S1, S2, and S3, which were mainly enriched for phytohormone signaling and phenylpropanoid metabolism. Phytohormone analysis indicated that IAA and CK jointly regulated root development, and *C. auriculatum* inhibited ETH synthesis and signaling to ensure the germination and expansion of tuberous roots. Chemical staining of lignin showed that in S1, lignified cells concentrated in the central xylem of root tuber. In S2, more lignified cells formed a ring structure separated from the central core. In S3, the vertical section of the root showed many rays connecting the xylem and phloem of *C. auriculatum* tuberous root. Besides, lignin content increased in S2 and decreased in S3, and the expression of lignin biosynthesis genes also showed a similar trend. With the development of *C. auriculatum* tuberous roots, the content of flavonoids gradually increased, and the expression of flavonoids biosynthesis genes also showed a similar trend. The expressions of rate-limiting genes suggested that *C. auriculatum* diverted the precursors to flavonoids by inhibiting lignin synthesis. Our results will aid in the investigations of phytohormones and phenylpropanoid biosynthesis in *C. auriculatum* tuber root development and may be helpful to improve the application value of *C. auriculatum*.

Declarations

Authors' contribution statement

Miao Sun: Conceptualization, Experiment, Software, Visualization, Writing-original draft preparation. **Zhi-Peng Zhu**: Experiment, Methodology. **Jian-Xiang Yu**: Methodology. **Ke-Xin Wu**: Experiment. **Yao-Xian Guo**: Methodology, Experiment. **Min Shen**: Conceptualization, Methodology, Resources. **Fang-Fang Liu**: Methodology, Experiment. **Xin-Hui Tang and Yi-Jun Kang**: Conceptualization, Methodology, Resources, Writing-reviewing and modifying, Funding acquisition. All authors have read and approved the manuscript.

Funding

This work was financed by the Open Project of Jiangsu Key Laboratory for Bioresources of Saline Soils (JKLBS2016002), National Natural Science Foundation of China (41977112), and Natural Science

Research of Jiangsu Higher Education Institutions of China (21KJB210007).

Declarations of interest

The authors declare that they have no known competing financial interests or personal relationships that could have appeared to influence the work reported in this paper.

Data Availability

The datasets generated during and analyzed during the current study are available from the corresponding author on reasonable request.

References

1. Ashburner M, Ball CA, Blake JA, Botstein D, Butler H, Cherry JM, Davis AP, Dolinski K, Dwight SS, Eppig JT, Harris MA, Hill DP, Issel-Tarver L, Kasarskis A, Lewis S, Matese JC, Richardson JE, Ringwald M, Rubin GM, Sherlock G (2000) Gene ontology: tool for the unification of biology. The Gene Ontology Consortium. Nat Genet 25:25–29. https://doi.org/10.1038/75556
2. Bailly C (2021) Anticancer properties of caudatin and related C-21 steroidal glycosides from Cynanchum plants. Steroids 172:108855. https://doi.org/10.1016/j.steroids.2021.108855
3. Bhargava A, Mansfield SD, Hall HC, Douglas CJ, Ellis BE (2010) MYB75 functions in regulation of secondary cell wall formation in the Arabidopsis inflorescence stem. Plant Physiol 154:1428–1438. https://doi.org/10.1104/pp.110.162735
4. Carbonnel S, Das D, Varshney K, Kolodziej MC, Villaécija-Aguilar JA, Gutjahr C (2020) The karrikin signaling regulator SMAX1 controls Lotus japonicus root and root hair development by suppressing ethylene biosynthesis. Proc Natl Acad Sci U S A 117:21757–21765. https://doi.org/10.1073/pnas.2006111117
5. Chai Z, Huang W, Zhao X, Wu H, Zeng X, Li C (2018) Preparation, characterization, antioxidant activity and protective effect against cellular oxidative stress of polysaccharide from Cynanchum auriculatum Royle ex Wight. Int J Biol Macromol 119:1068–1076. https://doi.org/10.1016/j.ijbiomac.2018.08.024
6. Chen S, Li X, Liu X, Wang N, An Q, Ye XM, Zhao ZT, Zhao M, Han Y, Ouyang KH, Wang WJ (2020) Investigation of Chemical Composition, Antioxidant Activity, and the Effects of Alfalfa Flavonoids on Growth Performance. Oxid Med Cell Longev 2020, 8569237. https://doi.org/10.1155/2020/8569237
7. Chen S, Zhou Y, Chen Y, Gu J (2018) fastp: an ultra-fast all-in-one FASTQ preprocessor. Bioinformatics 34:i884–i890. https://doi.org/10.1093/bioinformatics/bty560
8. Chen W-h, Zhang Z-z, Ban Y-f, Rahman K, Ye B-z, Sun X-l, Tan H-y, Zheng X-h, Liu H-y, Xu L-c, Yan B, Han T (2019) Cynanchum bungei Decne and its two related species for “Baishouwu”: A review on traditional uses, phytochemistry, and pharmacological activities. J Ethnopharmacol 243:112110. https://doi.org/10.1016/j.jep.2019.112110

9. Chen Y, Yi N, Yao SB, Zhuang J, Fu Z, Ma J, Yin S, Jiang X, Liu Y, Gao L, Xia T (2021) CsHCT-Mediated Lignin Synthesis Pathway Involved in the Response of Tea Plants to Biotic and Abiotic Stresses. J Agric Food Chem 69:10069–10081. https://doi.org/10.1021/acs.jafc.1c02771
10. Dai H, Fu M, Yang X, Chen Q (2016) Ethylene inhibited sprouting of potato tubers by influencing the carbohydrate metabolism pathway. J Food Sci Technol 53:3166–3174. https://doi.org/10.1007/s13197-016-2290-0
11. Deluc L, Bogs J, Walker AR, Ferrier T, Decendit A, Merillon JM, Robinson SP, Barrieu F (2008) The transcription factor VvMYB5b contributes to the regulation of anthocyanin and proanthocyanidin biosynthesis in developing grape berries. Plant Physiol 147:2041–2053. https://doi.org/10.1104/pp.108.118919
12. Dong NQ, Lin HX (2021) Contribution of phenylpropanoid metabolism to plant development and plant-environment interactions. J Integr Plant Biol 63:180–209. https://doi.org/10.1111/jipb.13054
13. Firon N, LaBonte D, Villordon A, Kfir Y, Solis J, Lapis E, Perlman TS, Doron-Faigenboim A, Hetzroni A, Althan L, Adani Nadir L (2013) Transcriptional profiling of sweetpotato (Ipomoea batatas) roots indicates down-regulation of lignin biosynthesis and up-regulation of starch biosynthesis at an early stage of storage root formation. BMC Genomics 14:460. https://doi.org/10.1186/1471-2164-14-460
14. Fischer U, Kucukoglu M, Helariutta Y, Bhalerao RP (2019) The Dynamics of Cambial Stem Cell Activity. Annu Rev Plant Biol 70:293–319. https://doi.org/10.1146/annurev-arplant-050718-100402
15. Fornalé S, Shi X, Chai C, Encina A, Irar S, Capellades M, Fuguet E, Torres JL, Rovira P, Puigdomènech P, Rigau J, Grotewold E, Gray J, Caparrós-Ruiz D (2010) ZmMYB31 directly represses maize lignin genes and redirects the phenylpropanoid metabolic flux. Plant J 64:633–644. https://doi.org/10.1111/j.1365-313X.2010.04363.x
16. Gámez-Arjona FM, Mérida Á (2021) Interplay Between the N-Terminal Domains of Arabidopsis Starch Synthase 3 Determines the Interaction of the Enzyme With the Starch Granule. Front Plant Sci 12:704161. https://doi.org/10.3389/fpls.2021.704161
17. Gao J, Cao X, Shi S, Ma Y, Wang K, Liu S, Chen D, Chen Q, Ma H (2016) Genome-wide survey of Aux/IAA gene family members in potato (Solanum tuberosum): Identification, expression analysis, and evaluation of their roles in tuber development. Biochem Biophys Res Commun 471:320–327. https://doi.org/10.1016/j.bbrc.2016.02.013
18. Gu L, Wu Y, Li M, Wang F, Li Z, Yuan F, Zhang Z (2021) Over-immunity mediated abnormal deposition of lignin arrests the normal enlargement of the root tubers of Rehmannia glutinosa under consecutive monoculture stress. Plant Physiol Biochem 165:36–46. https://doi.org/10.1016/j.plaphy.2021.05.010
19. Jang G, Lee JH, Rastogi K, Park S, Oh SH, Lee JY (2015) Cytokinin-dependent secondary growth determines root biomass in radish (Raphanus sativus L.). J Exp Bot 66:4607–4619. https://doi.org/10.1093/jxb/erv220
20. Jing H, Strader LC (2019) Interplay of Auxin and Cytokinin in Lateral Root Development. Int J Mol Sci 20:486. https://doi.org/10.3390/ijms20030486

21. Kolachevskaya OO, Alekseeva VV, Sergeeva LI, Rukavtsova EB, Getman IA, Vreugdenhil D, Buryanov YI, Romanov GA (2015) Expression of auxin synthesis gene tms1 under control of tuber-specific promoter enhances potato tuberization in vitro. J Integr Plant Biol 57:734–744. https://doi.org/10.1111/jipb.12314
22. Kondhare KR, Natarajan B, Banerjee AK (2020) Molecular signals that govern tuber development in potato. Int J Dev Biol 64:133–140. https://doi.org/10.1387/ijdb.190132ab
23. Kondhare KR, Patil AB, Giri AP (2021) Auxin: An emerging regulator of tuber and storage root development. Plant Sci 306:110854. https://doi.org/10.1016/j.plantsci.2021.110854
24. Li Y, Piao D, Zhang H, Woo MH, Lee JH, Moon DC, Lee SH, Chang HW, Son JK (2013) Quality assessment and discrimination of the roots of Cynanchum auriculatum and Cynanchum wilfordii by HPLC-UV analysis. Arch Pharm Res 36:335–344. https://doi.org/10.1007/s12272-013-0060-3
25. Liang M, Davis E, Gardner D, Cai X, Wu Y (2006) Involvement of AtLAC15 in lignin synthesis in seeds and in root elongation of Arabidopsis. Planta 224:1185–1196. https://doi.org/10.1007/s00425-006-0300-6
26. Liu J, Moore S, Chen C, Lindsey K (2017) Crosstalk Complexities between Auxin, Cytokinin, and Ethylene in Arabidopsis Root Development: From Experiments to Systems Modeling, and Back Again. Mol Plant 10:1480–1496. https://doi.org/10.1016/j.molp.2017.11.002
27. Liu Q, Luo L, Zheng L (2018) Lignins: Biosynthesis and Biological Functions in Plants. Int J Mol Sci 19:335. https://doi.org/10.3390/ijms19020335
28. Liu W, Feng Y, Yu S, Fan Z, Li X, Li J, Yin H (2021) The Flavonoid Biosynthesis Network in Plants. Int J Mol Sci 22:12824. https://doi.org/10.3390/ijms222312824
29. Livak KJ, Schmittgen TJM (2001) Analysis of relative gene expression data using real-time quantitative PCR and the 2-DDCt method. Methods 25:402–408. https://doi.org/10.1006/meth.2001.1262
30. Love MI, Huber W, Anders S (2014) Moderated estimation of fold change and dispersion for RNA-seq data with DESeq2. Genome Biol 15:550. https://doi.org/10.1186/s13059-014-0550-8
31. Lu KJ, Pfister B, Jenny C, Eicke S, Zeeman SC (2018) Distinct Functions of STARCH SYNTHASE 4 Domains in Starch Granule Formation. Plant Physiol 176:566–581. https://doi.org/10.1104/pp.17.01008
32. Ma J, Aloni R, Villordon A, Labonte D, Kfir Y, Zemach H, Schwartz A, Althan L, Firon N (2015) Adventitious root primordia formation and development in stem nodes of 'Georgia Jet' sweetpotato, Ipomoea batatas. Am J Bot 102:1040–1049. https://doi.org/10.3732/ajb.1400505
33. Mehdi R, Lamm CE, Bodampalli Anjanappa R, Müdsam C, Saeed M, Klima J, Kraner ME, Ludewig F, Knoblauch M, Gruissem W, Sonnewald U, Zierer W (2019) Symplasmic phloem unloading and radial post-phloem transport via vascular rays in tuberous roots of Manihot esculenta. J Exp Bot 70:5559–5573. https://doi.org/10.1093/jxb/erz297
34. Melis RJM, van Staden J (1985) Tuberization in Cassava (Manihot esculenta): Cytokinin and Abscisic Acid Activity in Tuberous Roots. J Plant Physiol 118:357–366.

https://doi.org/10.1016/S0176-1617(85)80195-4

35. Mir Derikvand M, Sierra JB, Ruel K, Pollet B, Do CT, Thévenin J, Buffard D, Jouanin L, Lapierre C (2008) Redirection of the phenylpropanoid pathway to feruloyl malate in Arabidopsis mutants deficient for cinnamoyl-CoA reductase 1. Planta 227:943–956. https://doi.org/10.1007/s00425-007-0669-x
36. Noh SA, Lee HS, Kim YS, Paek KH, Shin JS, Bae JM (2013) Down-regulation of the IbEXP1 gene enhanced storage root development in sweetpotato. J Exp Bot 64:129–142. https://doi.org/10.1093/jxb/ers236
37. Parhi B, Bharatiya D, Swain SK (2020) Application of quercetin flavonoid based hybrid nanocomposites: A review. Saudi Pharm J 28:1719–1732. https://doi.org/10.1016/j.jsps.2020.10.017
38. Park S, Kim DH, Yang JH, Lee JY, Lim SH (2020) Increased Flavonol Levels in Tobacco Expressing AcFLS Affect Flower Color and Root Growth. Int J Mol Sci 21:1011. https://doi.org/10.3390/ijms21031011
39. Pertea M, Pertea GM, Antonescu CM, Chang TC, Mendell JT, Salzberg SL (2015) StringTie enables improved reconstruction of a transcriptome from RNA-seq reads. Nat Biotechnol 33:290–295. https://doi.org/10.1038/nbt.3122
40. Qi LW, Gu XJ, Li P, Liang Y, Hao H, Wang G (2009) Structural characterization of pregnane glycosides from Cynanchum auriculatum by liquid chromatography on a hybrid ion trap time-of-flight mass spectrometer. Rapid Commun Mass Spectrom 23:2151–2160. https://doi.org/10.1002/rcm.4125
41. Qin H, He L, Huang R (2019a) The Coordination of Ethylene and Other Hormones in Primary Root Development. Front Plant Sci 10:874. https://doi.org/10.3389/fpls.2019.00874
42. Qin H, Huang R (2018) Auxin Controlled by Ethylene Steers Root Development. Int J Mol Sci 19:3656. https://doi.org/10.3390/ijms19113656
43. Qin H, Wang J, Chen X, Wang F, Peng P, Zhou Y, Miao Y, Zhang Y, Gao Y, Qi Y, Zhou J, Huang R (2019b) Rice OsDOF15 contributes to ethylene-inhibited primary root elongation under salt stress. New Phytol 223:798–813. https://doi.org/10.1111/nph.15824
44. Ralph J, Lapierre C, Boerjan W (2019) Lignin structure and its engineering. Curr Opin Biotechnol 56:240–249. https://doi.org/10.1016/j.copbio.2019.02.019
45. Robinson MD, McCarthy DJ, Smyth GK (2010) edgeR: a Bioconductor package for differential expression analysis of digital gene expression data. Bioinformatics 26:139–140. https://doi.org/10.1093/bioinformatics/btp616
46. Roosjen M, Paque S, Weijers D (2018) Auxin Response Factors: output control in auxin biology. J Exp Bot 69:179–188. https://doi.org/10.1093/jxb/erx237
47. Rüscher D, Corral JM, Carluccio AV, Klemens PAW, Gisel A, Stavolone L, Neuhaus HE, Ludewig F, Sonnewald U, Zierer W (2021) Auxin signaling and vascular cambium formation enable storage metabolism in cassava tuberous roots. J Exp Bot 72:3688–3703. https://doi.org/10.1093/jxb/erab106

48. Schilmiller AL, Stout J, Weng JK, Humphreys J, Ruegger MO, Chapple C (2009) Mutations in the cinnamate 4-hydroxylase gene impact metabolism, growth and development in Arabidopsis. Plant J 60:771–782. https://doi.org/10.1111/j.1365-313X.2009.03996.x
49. Schwall GP, Safford R, Westcott RJ, Jeffcoat R, Tayal A, Shi YC, Gidley MJ, Jobling SA (2000) Production of very-high-amylose potato starch by inhibition of SBE A and B. Nat Biotechnol 18:551–554. https://doi.org/10.1038/75427
50. Shi J, Yan X, Sun T, Shen Y, Shi Q, Wang W, Bao M, Luo H, Nian F, Ning G (2022) Homeostatic regulation of flavonoid and lignin biosynthesis in phenylpropanoid pathway of transgenic tobacco. Gene 809:146017. https://doi.org/10.1016/j.gene.2021.146017
51. Singh V, Zemach H, Shabtai S, Aloni R, Yang J, Zhang P, Sergeeva L, Ligterink W, Firon N (2020) Proximal and Distal Parts of Sweetpotato Adventitious Roots Display Differences in Root Architecture, Lignin, and Starch Metabolism and Their Developmental Fates. Front Plant Sci 11:609923. https://doi.org/10.3389/fpls.2020.609923
52. Sojikul P, Saithong T, Kalapanulak S, Pisuttinusart N, Limsirichaikul S, Tanaka M, Utsumi Y, Sakurai T, Seki M, Narangajavana J (2015) Genome-wide analysis reveals phytohormone action during cassava storage root initiation. Plant Mol Biol 88:531–543. https://doi.org/10.1007/s11103-015-0340-z
53. Sun M, Yang XL, Zhu ZP, Xu QY, Wu KX, Kang YJ, Wang H, Xiong AS (2021) Comparative transcriptome analysis provides insight into nitric oxide suppressing lignin accumulation of postharvest okra (Abelmoschus esculentus L.) during cold storage. Plant Physiol Biochem 167:49–67. https://doi.org/10.1016/j.plaphy.2021.07.029
54. Sun W, Ma Z, Chen H, Liu M (2019) MYB Gene Family in Potato (Solanum tuberosum L.): Genome-Wide Identification of Hormone-Responsive Reveals Their Potential Functions in Growth and Development. Int J Mol Sci 20:4878. https://doi.org/10.3390/ijms20194847
55. Thévenin J, Pollet B, Letarnec B, Saulnier L, Gissot L, Maia-Grondard A, Lapierre C, Jouanin L (2011) The simultaneous repression of CCR and CAD, two enzymes of the lignin biosynthetic pathway, results in sterility and dwarfism in Arabidopsis thaliana. Mol Plant 4:70–82. https://doi.org/10.1093/mp/ssq045
56. Uchikura T, Tanaka H, Sugiwaki H, Yoshimura M, Sato-Masumoto N, Tsujimoto T, Uchiyama N, Hakamatsuka T, Amakura Y (2018) Preliminary Quality Evaluation and Characterization of Phenolic Constituents in Cynanchi Wilfordii Radix. Molecules 23:656. https://doi.org/10.3390/molecules23030656
57. Utsumi Y, Tanaka M, Utsumi C, Takahashi S, Matsui A, Fukushima A, Kobayashi M, Sasaki R, Oikawa A, Kusano M, Saito K, Kojima M, Sakakibara H, Sojikul P, Narangajavana J, Seki M (2020) Integrative omics approaches revealed a crosstalk among phytohormones during tuberous root development in cassava. Plant Mol Biol 109:249–269. https://doi.org/10.1007/s11103-020-01033-8
58. Utsumi Y, Utsumi C, Tanaka M, Takahashi S, Okamoto Y, Ono M, Nakamura Y, Seki M (2021) Suppressed expression of starch branching enzyme 1 and 2 increases resistant starch and amylose

content and modifies amylopectin structure in cassava. Plant Mol Biol 108:413–427. https://doi.org/10.1007/s11103-021-01209-w

59. Vanholme R, Storme V, Vanholme B, Sundin L, Christensen JH, Goeminne G, Halpin C, Rohde A, Morreel K, Boerjan W (2012) A systems biology view of responses to lignin biosynthesis perturbations in Arabidopsis. Plant Cell 24:3506–3529. https://doi.org/10.1105/tpc.112.102574
60. Villordon AQ, Ginzberg I, Firon N (2014) Root architecture and root and tuber crop productivity. Trends Plant Sci 19:419–425. https://doi.org/10.1016/j.tplants.2014.02.002
61. Vogt T (2010) Phenylpropanoid biosynthesis. Mol Plant 3:2–20. https://doi.org/10.1093/mp/ssp106
62. Wang H, Yang J, Zhang M, Fan W, Firon N, Pattanaik S, Yuan L, Zhang P (2016) Altered Phenylpropanoid Metabolism in the Maize Lc-Expressed Sweet Potato (Ipomoea batatas) Affects Storage Root Development. Sci Rep 6:18645. https://doi.org/10.1038/srep18645
63. Wang L, Lu W, Ran L, Dou L, Yao S, Hu J, Fan D, Li C, Luo K (2019) R2R3-MYB transcription factor MYB6 promotes anthocyanin and proanthocyanidin biosynthesis but inhibits secondary cell wall formation in Populus tomentosa. Plant J 99:733–751. https://doi.org/10.1111/tpj.14364
64. Wang P, Lu S, Xie M, Wu M, Ding S, Khaliq A, Ma Z, Mao J, Chen B (2020) Identification and expression analysis of the small auxin-up RNA (SAUR) gene family in apple by inducing of auxin. Gene 750:144725. https://doi.org/10.1016/j.gene.2020.144725
65. Wu CD, Zhang M, He MT, Gu MF, Lin M, Zhang G (2019) Selection of solvent for extraction of antioxidant components from Cynanchum auriculatum, Cynanchum bungei, and Cynanchum wilfordii roots. Food Sci Nutr 7:1337–1343. https://doi.org/10.1002/fsn3.967
66. Yao Y, Geng MT, Wu XH, Sun C, Wang YL, Chen X, Shang L, Lu XH, Li Z, Li RM, Fu SP, Duan RJ, Liu J, Hu XW, Guo JC (2017) Identification, Expression, and Functional Analysis of the Fructokinase Gene Family in Cassava. Int J Mol Sci 18:2398. https://doi.org/10.3390/ijms18112398
67. Zhang M, Wang D, Li B (2019) Neuroprotection of two C21 steroidal glycosides from Cynanchum auriculatum against H2O2-induced damage on PC12 cells. Nat Prod Res 35:1752–1755. https://doi.org/10.1080/14786419.2019.1636241
68. Zhang X, Shan L, Huang H, Yang X, Liang X, Xing A, Huang H, Liu X, Su J, Zhang W (2009) Rapid identification of acetophenones in two Cynanchum species using liquid chromatography-electrospray ionization tandem mass spectrometry. J Pharm Biomed Anal 49:715–725. https://doi.org/10.1016/j.jpba.2009.01.009
69. Zhao H, Ma B, Duan KX, Li XK, Lu X, Yin CC, Tao JJ, Wei W, Zhang WK, Xin PY, Lam M, Chu S, Shui JF, Chen GH, Zhang SY J.S., 2020. The GDSL Lipase MHZ11 Modulates Ethylene Signaling in Rice Roots.Plant Cell32,1626–1643. https://doi.org/10.1105/tpc.19.00840
70. Zhou Y, Li Y, Gong M, Qin F, Xiao D, Zhan J, Wang A, He L (2021) Regulatory mechanism of GA(3) on tuber growth by DELLA-dependent pathway in yam (Dioscorea opposita). Plant Mol Biol 106:433–448. https://doi.org/10.1007/s11103-021-01163-7
71. Zierer W, Rüscher D, Sonnewald U, Sonnewald S (2021) Tuber and Tuberous Root Development. Annu Rev Plant Biol 72:551–580. https://doi.org/10.1146/annurev-arplant-080720-084456

72. Zou X, Long J, Zhao K, Peng A, Chen M, Long Q, He Y, Chen S (2019) Overexpressing GH3.1 and GH3.1L reduces susceptibility to Xanthomonas citri subsp. citri by repressing auxin signaling in citrus (Citrus sinensis Osbeck). PLoS ONE 14:e0220017. https://doi.org/10.1371/journal.pone.0220017

Figures

Figure 1

Annual *C. auriculatum* root tubers at three development stages. (A) S1 represented root tuber forming stage, S2 represented root tuber thickening stage, and S3 represented root tuber harvest stage. (B) The average root length and average root weight of *C. auriculatum* root tubers at three development stages.

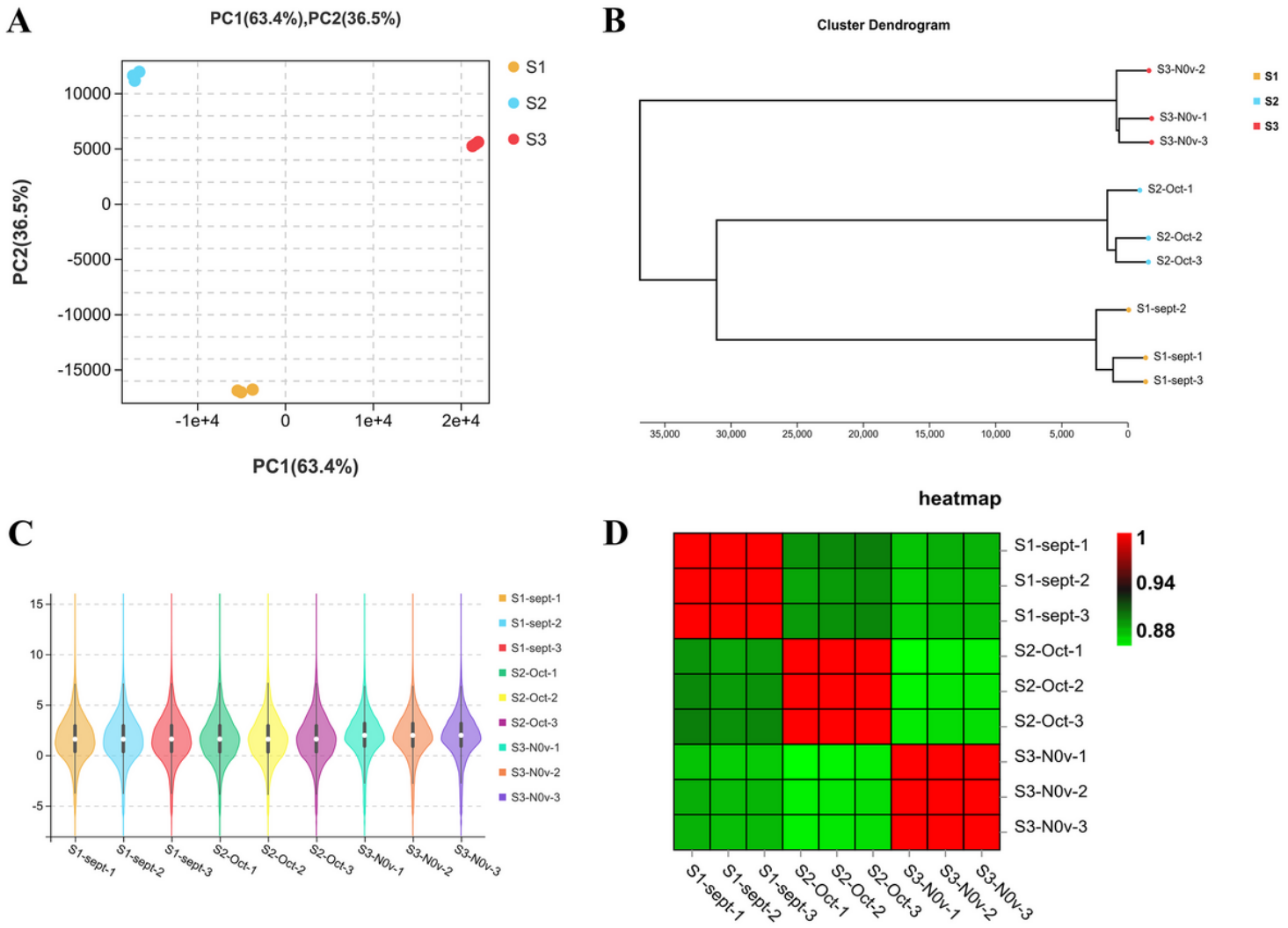

Figure 2

The sample relationship analysis of *C. auriculatum* root tuber. (A) PCA, the abscissa represented the first principal component (PC1), the ordinate represented the second principal component (PC2), and different comparison groups were represented by different colors. (B) Sample clustering analysis, the abscissa represented the Euclidean distance between samples, and each branch represented a sample. (C) Violin plot, which showed the data density at any location for all genes in the sample, the white dots represented the median, and the black rectangles were the range from the lower quartile (Q1) to the upper quartile (Q3). (D) Correlation heat map, the abscissa and ordinate represented each sample, respectively, and the shade of color indicated the magnitude of the correlation coefficient between the two samples.

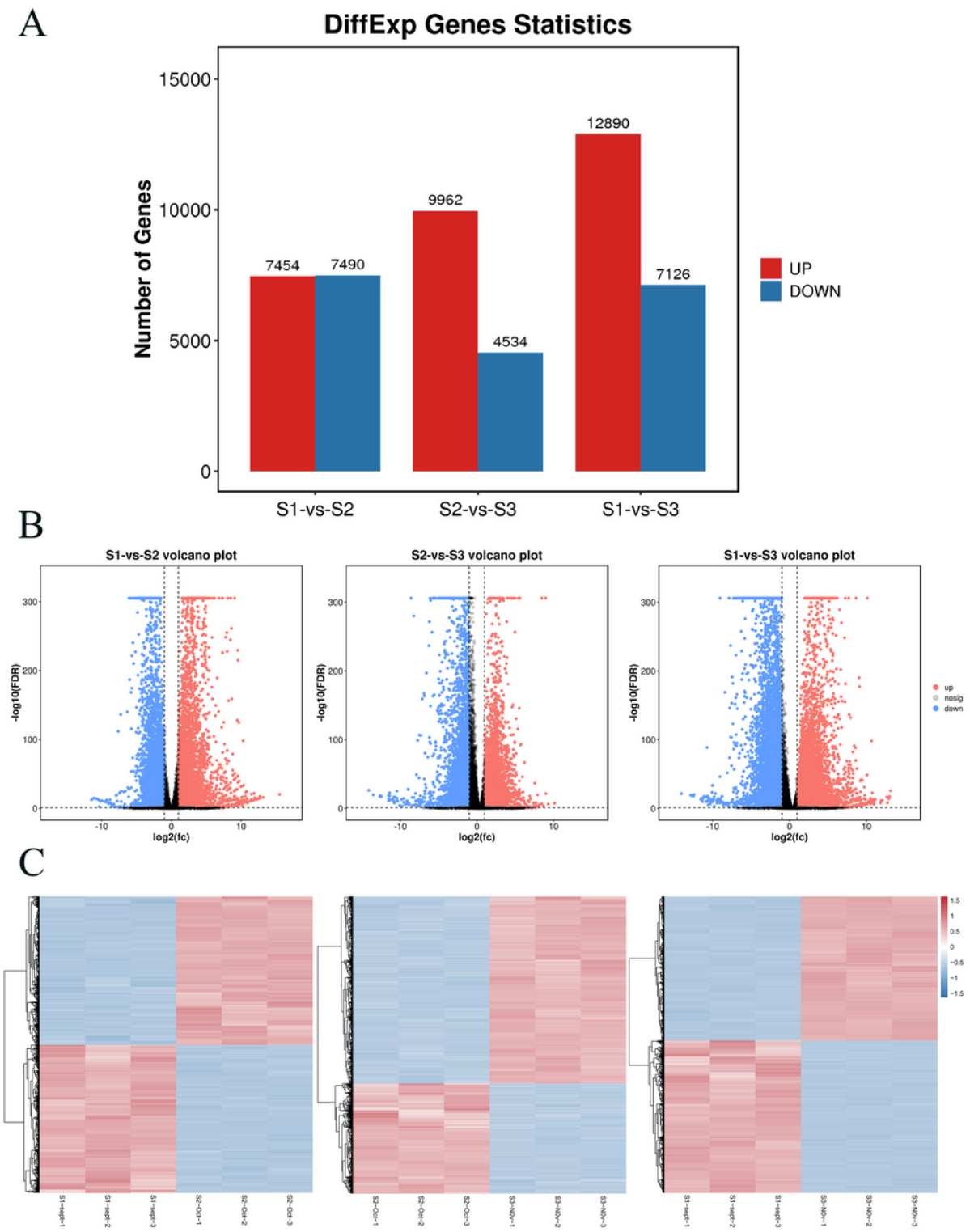

Figure 3

DEGs enrichment analysis of *C. auriculatum* tuberous root during development, including (A) DEGs statistics among the groups of S1, S2, and S3. (B) difference comparison volcano plot among the groups of S1, S2, and S3. (C) difference comparison cluster heatmap between three biological replicates at three development stages. (D) Venn diagram of DEGs among the groups of S1, S2, and S3.

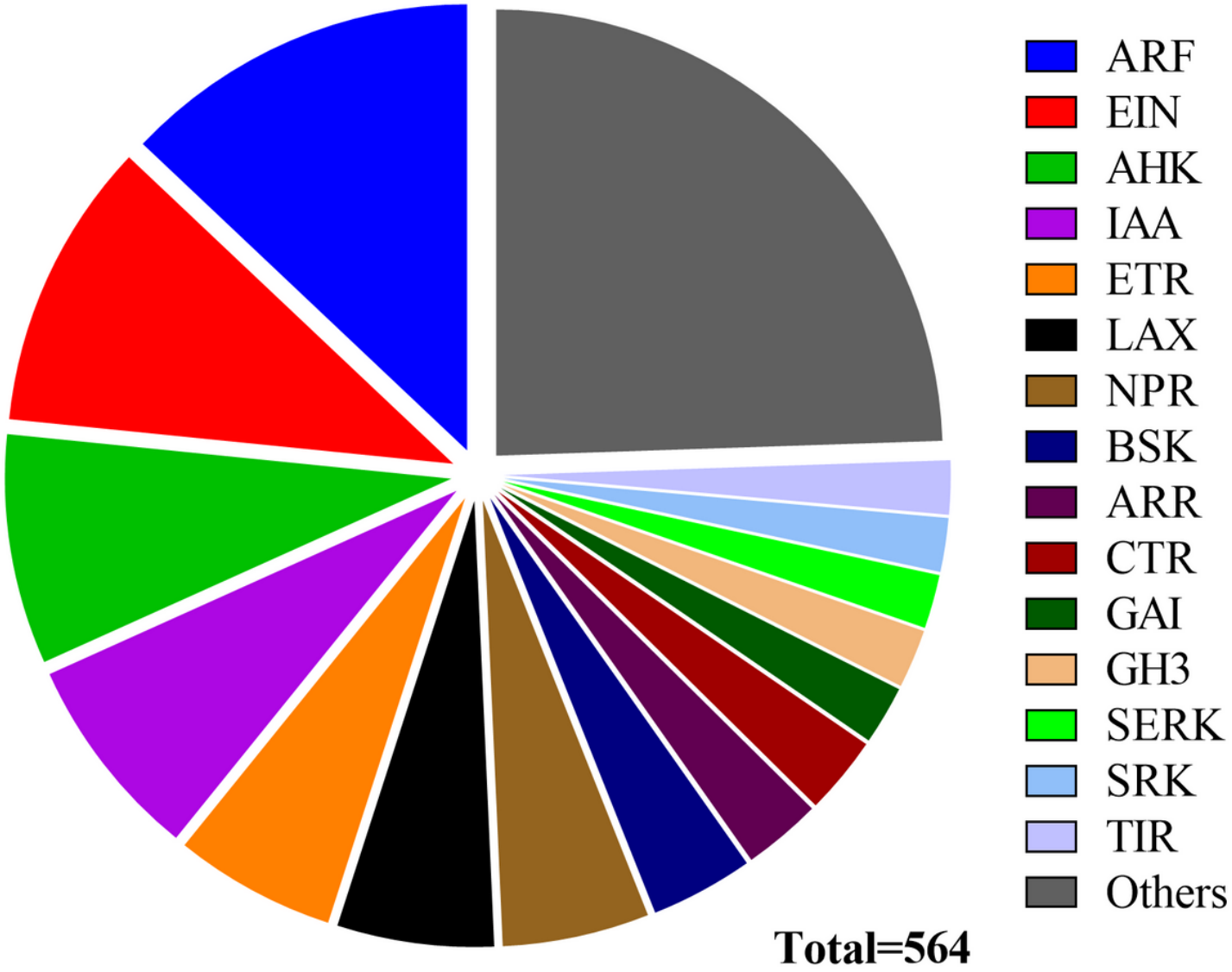

Figure 4

Overview of the distribution of phytohormone families that were differential expressed during development.

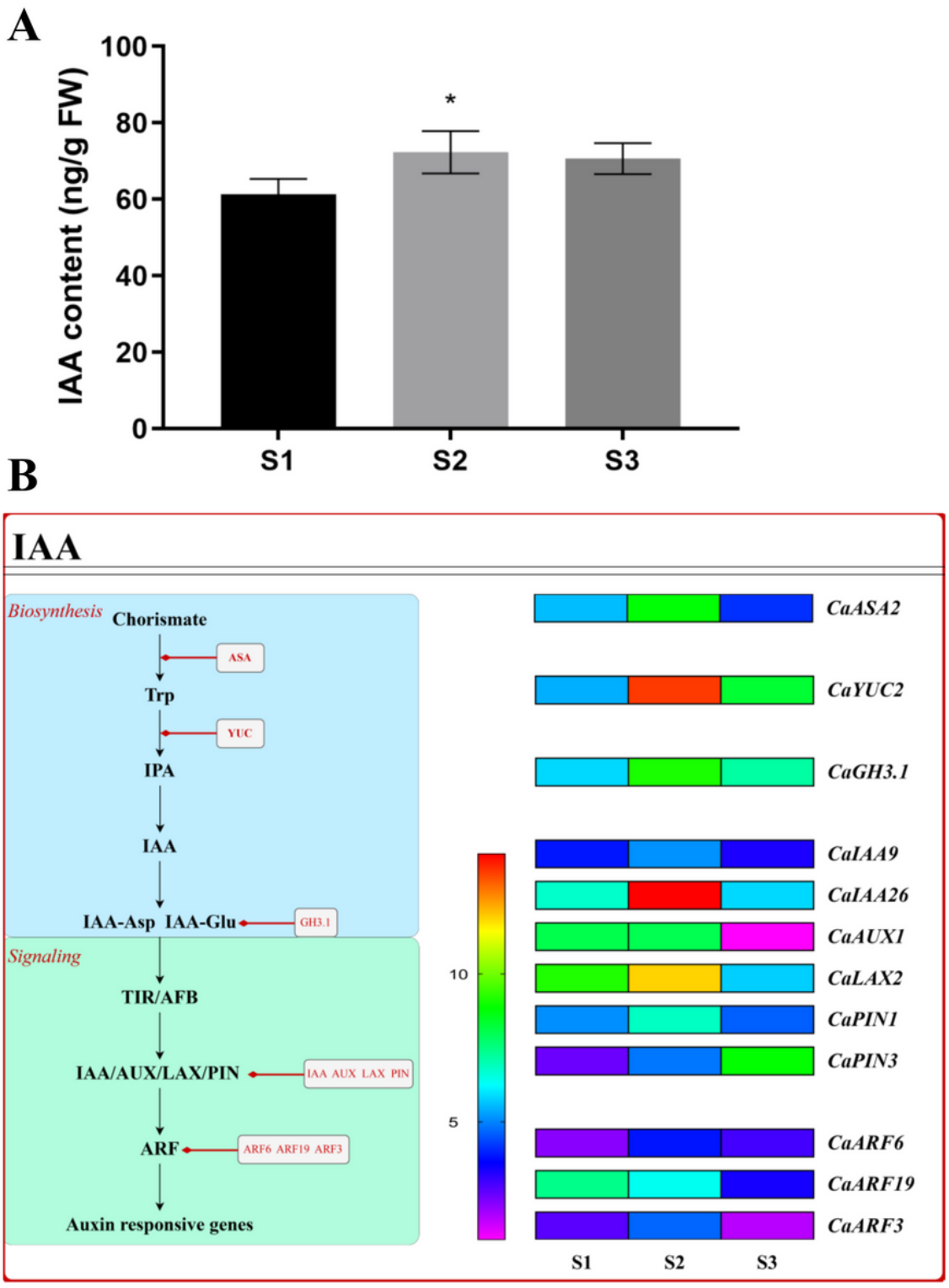

Figure 5

The IAA metabolic mechanism of *C. auriculatum* tuberous root during development. (A) IAA content of *C. auriculatum* tuberous root at the stages of S1, S2, and S3. (B) Differential expression profiles of genes involved in IAA biosynthesis, transport, and signaling at the stages of S1, S2, and S3.

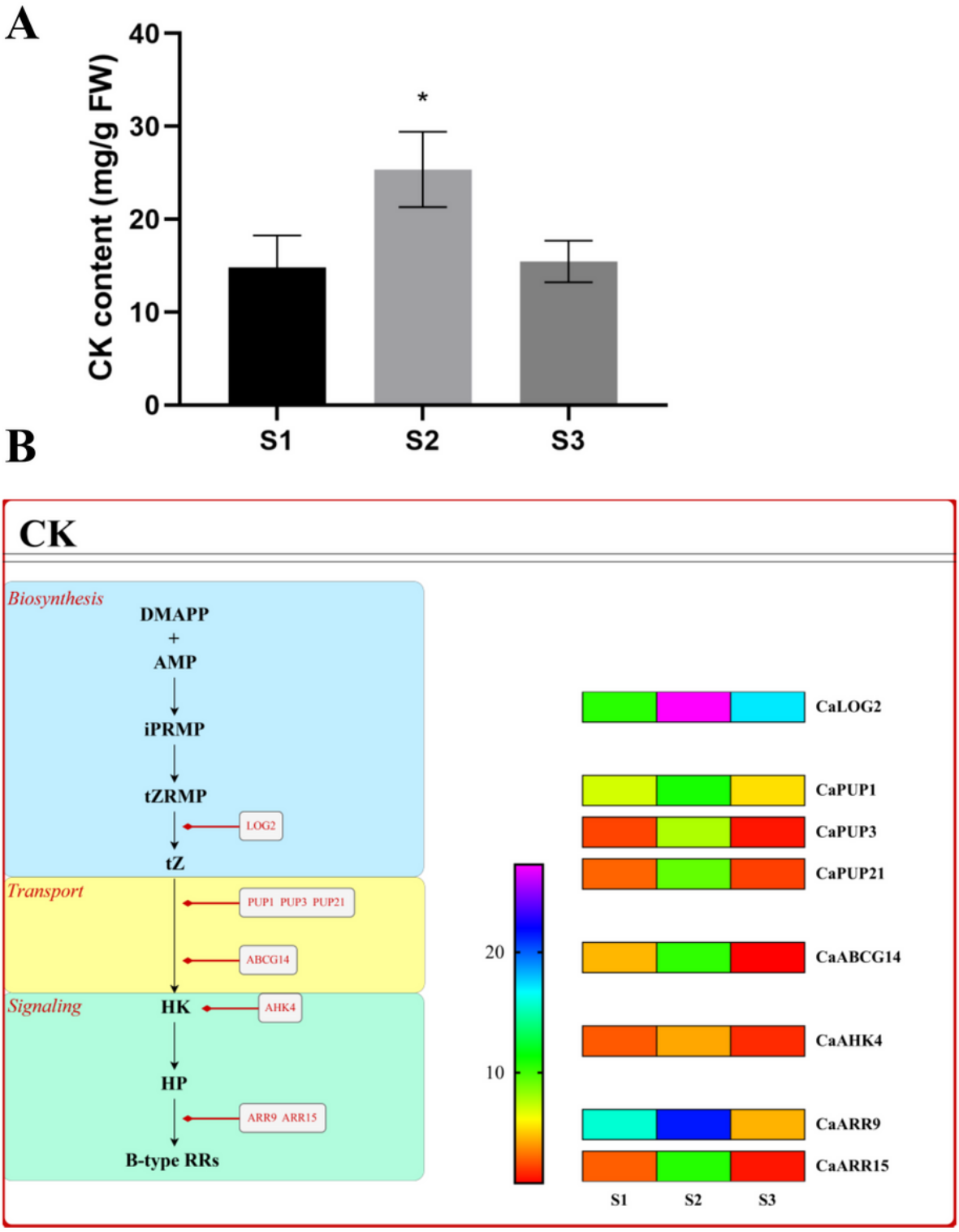

Figure 6

The CK metabolic mechanism of *C. auriculatum* tuberous root during development. (A) CK content of *C. auriculatum* tuberous root at the stages of S1, S2, and S3. (B) Differential expression profiles of genes involved in CK biosynthesis, transport, and signaling at the stages of S1, S2, and S3.

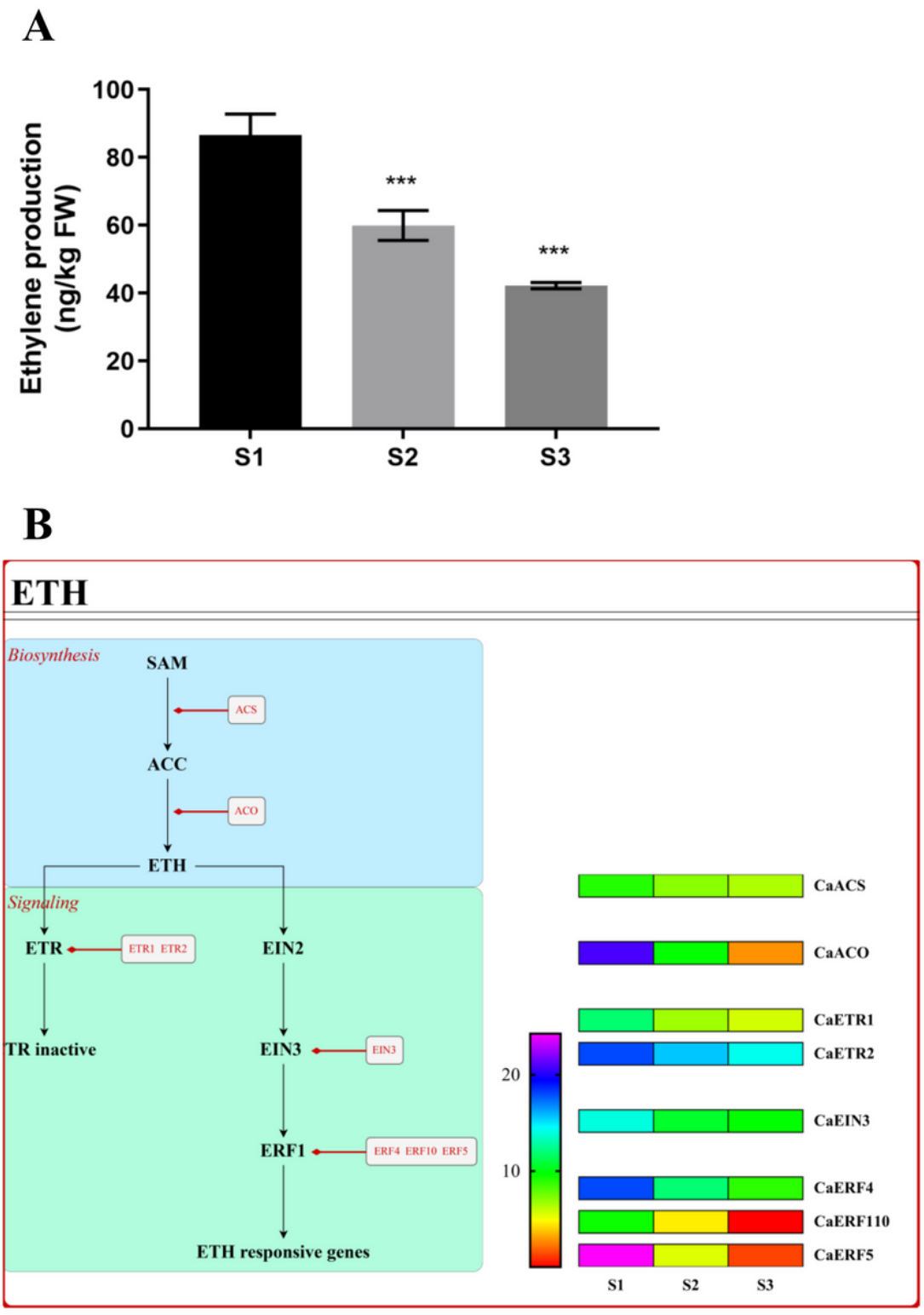

Figure 7

The ETH metabolic mechanism of *C. auriculatum* tuberous root during development. (A) ETH content of *C. auriculatum* tuberous root at the stages of S1, S2, and S3. (B) Differential expression profiles of genes involved in ETH biosynthesis and signaling at the stages of S1, S2, and S3.

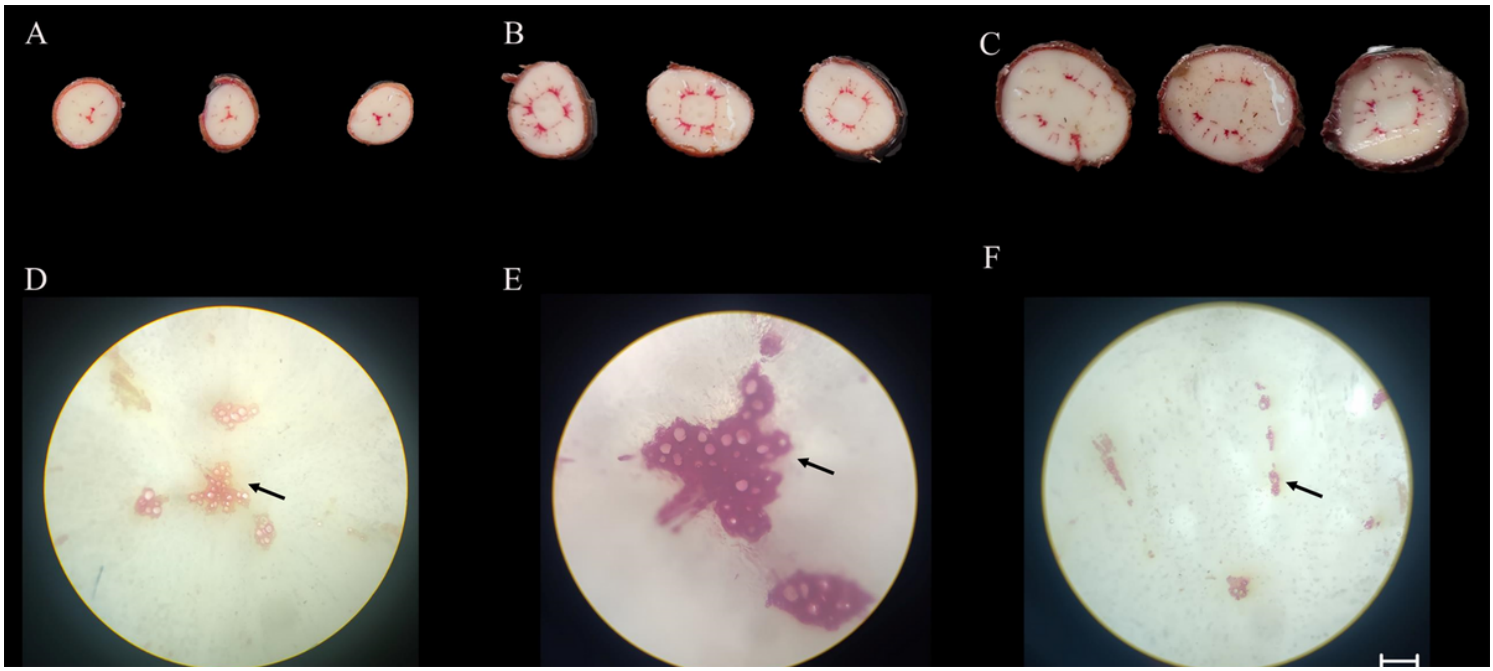

Figure 8

Lignified tissue phenotype in *C. auriculatum* tuberous roots based on chemical staining. (A) and (D) represented lignified tissue and cell of S1, (B) and (E) represented lignified tissue and cell of S2, (C) and (F) represented lignified tissue and cell of S3. Scale bar represented 100 μm.

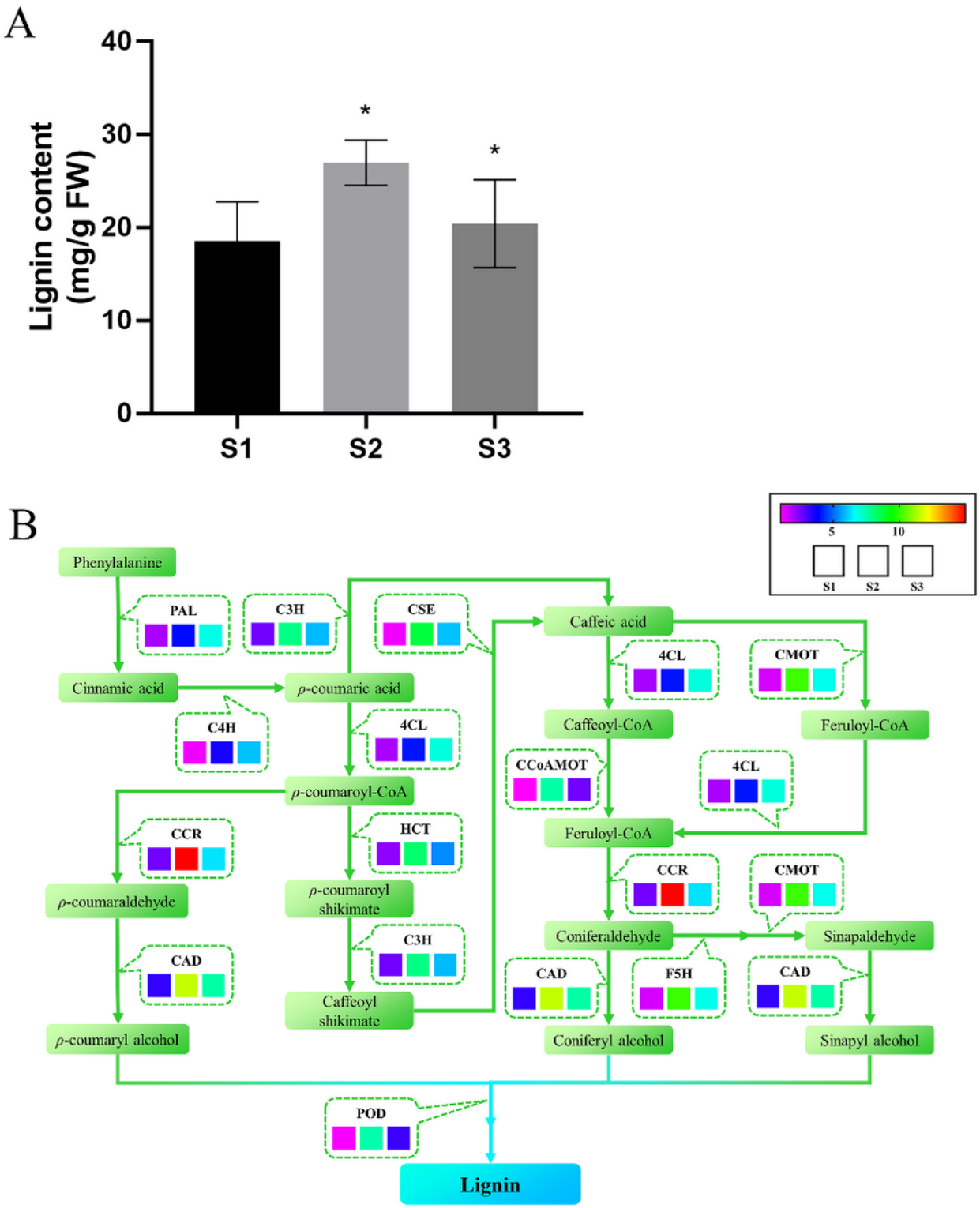

Figure 9

The lignin biosynthesis mechanism of *C. auriculatum* tuberous root during development. (A) The lignin content of *C. auriculatum* tuberous root at the stages of S1, S2, and S3. (B) Differential expression profiles of structural genes involved in the lignin biosynthesis pathway of *C. auriculatum* tuberous root at the stages of S1, S2, and S3.

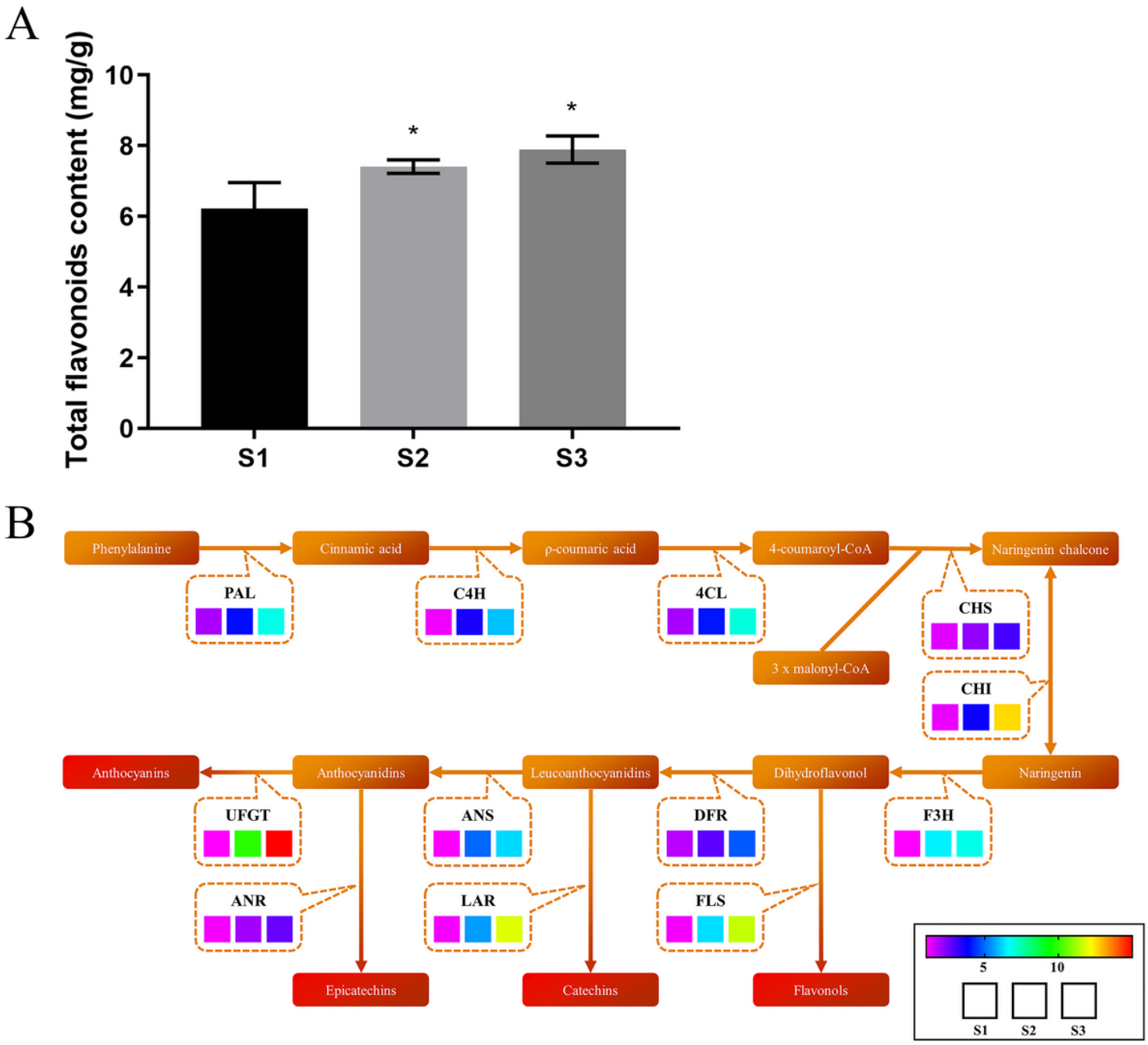

Figure 10

The flavonoids biosynthesis mechanism of *C. auriculatum* tuberous root during development. (A) Total flavonoids content of *C. auriculatum* tuberous root at the stages of S1, S2, and S3. (B) Differential expression profiles of structural genes involved in the flavonoids biosynthesis pathway of *C. auriculatum* tuberous root at the stages of S1, S2, and S3.

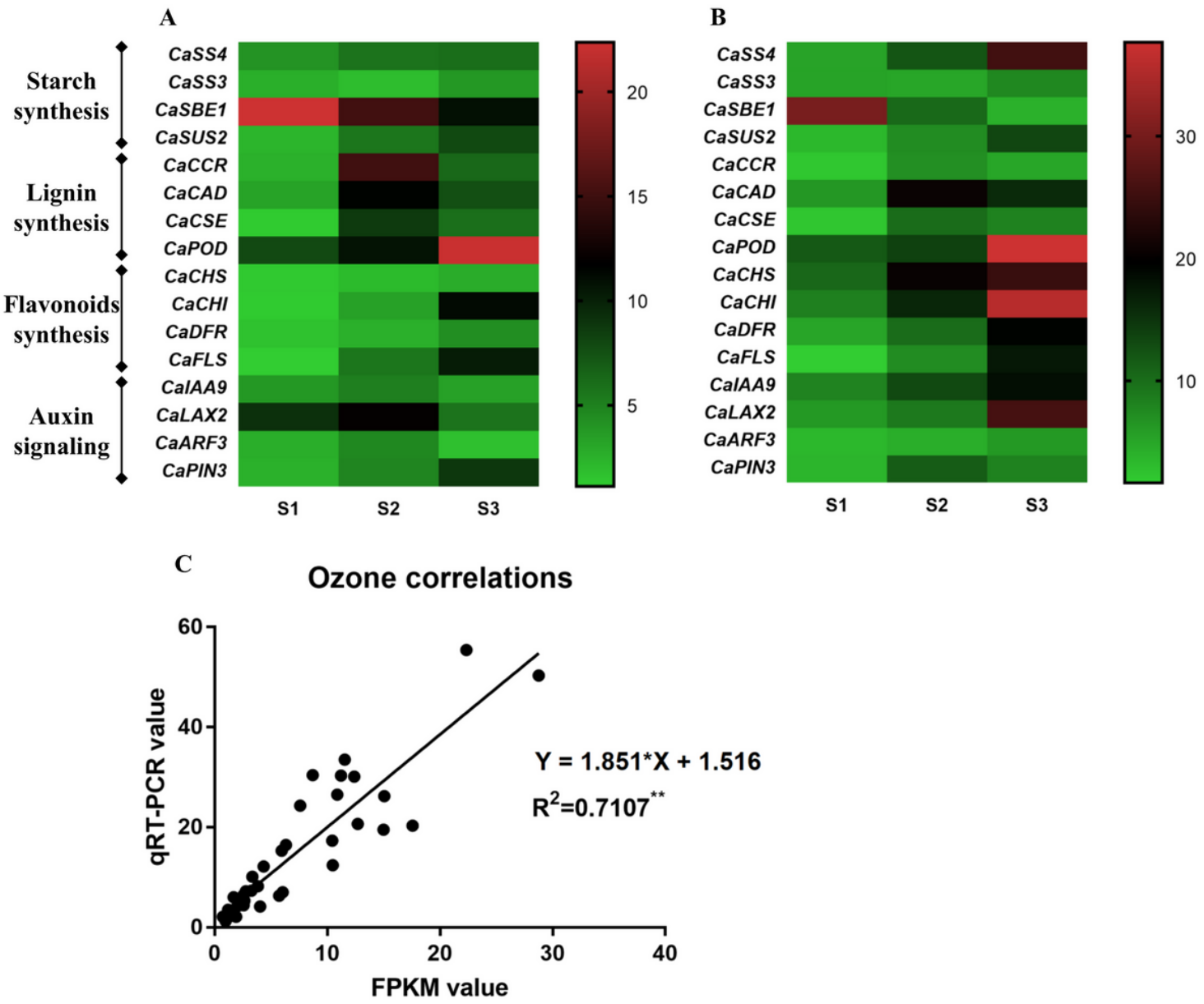

Figure 11

Expression level analysis of DEGs, which were related to starch metabolism, lignin metabolism, flavonoid metabolism, and auxin transduction, respectively, between RNA-Seq and qRT-PCR. (A) Heatmap of expression levels of the sixteen DEGs in RNA-Seq. (B) Heatmap of relative expression levels of the sixteen DEGs in qRT-PCR. (C) Ozone correlation analysis of expression levels of the sixteen DEGs in RNA-Seq and qRT-PCR.

Supplementary Files

This is a list of supplementary files associated with this preprint. Click to download.

- Supplementaryfiles.docx